UNCLASSIFIED

AD NUMBER

AD856679

NEW LIMITATION CHANGE

TO

Approved for public release, distribution unlimited

FROM

Distribution authorized to U.S. Gov't. agencies and their contractors; Administrative/Operational Use; Jun 1969. Other requests shall be referred to Naval Air Systems Command, Washington, DC 20360.

AUTHORITY

US Naval Air Systems Command ltr dtd 26 Oct 1971

THIS PAGE IS UNCLASSIFIED

MICROSTRUCTURE STUDIES OF POLYCRYSTALLINE OXIDES

SUMMARY REPORT

25 May 1968 to 24 June 1969

Contract N00019-68-C-0108

AVATD-0121-69-CR

Prepared for

U.S. Naval Air Systems
Washington 25, D.C.

Prepared by

W.H. Rhodes
P.F. Jahn
P.L. Burnett

AVCO CORPORATION
Applied Technology Division
Lowell, Massachusetts 01851

78

MICROSTRUCTURE STUDIES OF POLYCRYSTALLINE OXIDES

SUMMARY REPORT

25 May 1968 to 24 June 1969

Contract N00019-68-C-0108

AVATD-0121-69-CR

Prepared for

U.S. Naval Air Systems
Washington 25, D.C.

Approved by

T. Vasilos
T. Vasilos

Prepared by

W.H. Rhodes
P.F. Jahn
P.L. Burnett

AVCO CORPORATION
Applied Technology Division
Lowell, Massachusetts 01851

THIS DOCUMENT IS SUBJECT TO SPECIAL EXPORT CONTROLS AND EACH TRANSMITTAL TO FOREIGN GOVERNMENTS OR FOREIGN NATIONALS MAY BE MADE ONLY WITH THE PRIOR APPROVAL OF COMMANDER, NAVAL AIR SYSTEMS COMMAND, AIR_____, WASHINGTON, D.C. 20360

52032R

FOREWORD

This report was prepared by the Applied Technology Division of Avco Corporation under U.S. Navy Contract N00019-68-C-0108, entitled, Microstructure Studies of Polycrystalline Oxides."

The work was administered under the direction of the U.S. Department of the Navy, Air Systems Command, with Mr. Charles F. Bersch, Code AIR-52032A, acting as Project Engineer.

This report covers work conducted from 29 May 1968 to 24 June 1969.

The writers are pleased to acknowledge the contributions of the following individuals to this program; R. Gardner and P. Fuce for ceramographic preparation, P. Daniels, R. Martineau and J. Centorino for materials preparation. C.L. Houck for electron microscopy, R.M. Haag and P. Berneburg for x-ray studies, and R.M. Haag, T. Vasilos, R.M. Cannon and J. Niesse for useful discussions.

ABSTRACT

Dead load-time to failure studies on polycrystalline MgO exhibited a decreasing load bearing capacity with time which was interpreted by the Charles and Hillig stress corrosion model. The possibility of a mechanical model similar to that invoked for metals was considered and not ruled out.

Chemical polishing of polycrystalline Al_2O_3 was accomplished. but mechanical tests failed to show a statistically valid strength improvement. Only a thermally etched surface from an earlier study exhibited a pronounced surface sensitivity to fracture strength, and dry testing conditions were required to unequivocally demonstrate this effect.

Two new grades of high purity Al_2O_3 and MgO powders were fabricated, and mechanical testing of the Al_2O_3 showed equivalent brittle strengths and increased creep resistance when compared with less pure material with an equivalent microstructure. The explanation for the creep resistance may be either a slight increase in grain size which accompanied the test or decreased diffusivity due to the increased purity. Preliminary grain growth studies on high purity MgO indicate a normal grain growth behavior, but about an order of magnitude slower rate than 99.4% MgO.

Press forging of polycrystalline Al_2O_3 was directed toward solving the engineering and process control problems or forging material with a high in-line optical transmission. Considerable progress has been made although the desired properties have not yet been obtained.

TABLE OF CONTENTS

TABLE OF CONTENTS (Concl'd)

LIST OF ILLUSTRATIONS

LIST OF ILLUSTRATIONS (Concl'd)

LIST OF TABLES

I. INTRODUCTION

This study was concerned with the effects of microstructure and chemistry on the physico-mechanical properties of oxide ceramics.

Earlier studies[1,2,3] on the effect of surface structure and environment on the brittle mechanical properties of alumina and magnesia were continued. It had been demonstrated that moderate strain rate tests on magnesia did not exhibit stress corrosion behavior. Dead load-time to failure tests were conducted to investigate this point more fully. In addition, bend tests on chemically polished alumina were conducted to complete the range of surface structures tested for this material.

Over the last several years[2,3] a number of potential high purity alumina (99.9% cations) and magnesia powders have been screened for purity, powder physical characteristics and ease of fabrication to a uniform microstructure. The work to be reported consisted of continued fabrication of one selected powder for both magnesia and alumina, low and high temperature mechanical properties on alumina, and grain growth of magnesia. The properties obtained are compared with standard grades of alumina and magnesia.

Polycrystalline alumina was previously press-forged to height reductions of > 50% without loss of structural integrity.[2,3] Strengths were equivalent to hot pressed material, and were relatively insensitive to grain size up to 10 microns. Strength measurements to larger grain sizes are now reported. The major emphasis in the press forging effort was placed on understanding the engineering and physical ceramics of the deformation and recrystallization phenomena. The production of transparent alumina with high in-line transparency was the major goal to which the study was directed.[4]

II. EFFECT OF SURFACE CONDITION AND ATMOSPHERE ON THE FRACTURE STRENGTH OF MAGNESIA AND ALUMINA

A. General

This subject has been under study for several years.[1,2,3] A review of the literature revealed that the clearest example of strength sensitivity to surface condition was for glass, where there is general agreement that pre-existing microscopic Griffith[5] surface cracks act as stress concentrators leading to crack propagation at 10^{-2} to 10^{-4} of the theoretical strength of these materials. For very perfect surfaces, strengths ~ 0.8 of the 3.4 mpsi estimated theoretical strength have been obtained in fused quartz.[5,6] Flame polished sapphire has withstood stress levels of 3 mpsi at -196°C without failure,[7] but in the case of brittle crystalline material, the influence of pre-existing flaws on the fracture stress, the crack nucleation mechanism and the crack propagation mechanism are significant points of current research and dispute.

The results on MgO as of the beginning of the current program led to the conclusion that: 1) stress corrosion did not occur in MgO at room temperature at testing strain rates in the order of 5×10^{-3}/min., 2) room temperature fractures were nucleated by mobile dislocations; hence, high strengths were obtained in both air and argon for annealed specimens. Thus, the room temperature strength was not particularly sensitive to the initial crack length although it was not possible to say whether it was strictly due to the Griffith criteria or if the dislocation mechanism of Clarke et al[8] was dominant. The fact that the mechanical polished samples which certainly contained fresh dislocations showed significantly higher strengths suggested, however, that the classic Griffith relation holds at 77°K, rather than a dislocation crack nucleation process.

In polycrystalline Al_2O_3 it was concluded that: 1) stress corrosion results in a strength reduction to between 0.65 - 0.83 of the strength value at room temperature for "dry" moderate strain rate tests, 2) none of the surface finishes obtained were sufficiently perfect to prevent stress corrosion, 3) liquid N_2 or dry argon at 23°C suppressed stress corrosion, but only 30% strength increases were obtained for various polished and annealed surfaces. An air annealed surface tested at 77°K did exhibit a 44% strength increase over an as-ground surface, thus leading to the conclusion that this was the most efficient means of blunting surface flaws, 4) it was concluded that Griffith type surface flaws were controlling fracture strengths at both 77°K and 296°K. A switch over in mechanism to dislocation nucleated fracture at 296°K was not unequivocally discounted, but the results did not lend support to this school of thought.

The work reported in the following section was aimed at examining the question of stress corrosion in MgO by classic dead load-time to failure test, and to study the effect of one more surface condition (chemically polished) on the fracture strength of Al_2O_3.

B. Experimental Procedure

1. Specimen Preparation

Samples were vacuum hot pressed to a density of greater than 99% of theoretical density and grain size of from 1 to 10 microns. Linde A 99.9% aluminum oxide and Fisher Electronic Grade 99.4% magnesium oxide were used as starting powder. Unlike the previous Al_2O_3 tested, the billet prepared for this year's program contained ¼% MgO.

2. Surface Treatments

The MgO tests were conducted on 500 grit diamond ground surfaces. This results in a surface of moderate roughness showing evidence for surface cracks and grain pull-out (Figure 2.1). The center line average (Talysurf) surface roughness was 33.6 micro-inches.

Considerable effort was expended in reproducing and refining the Al_2O_3 chemical polishing treatment developed by Tomilovskii[9] for single crystals and King[10] for polycrystals. Fused borax was the polishing media. A 200 cc platinum crucible was isothermally held at 825°C. A cradle made from Pt-Rh wire contained the mechanically polished bend specimen in such a manner that the gage length of the tensile surface was not in contact with the wire cradle. The specimen was then lowered slowly into the bath and agitated in a non-concentric manner for 20 minutes. After slow cooling, the borax was removed by washing in concentrated HCl. The surface obtained is illustrated in Figure 2.2. The center line average surface roughness was 7 micro-inches.

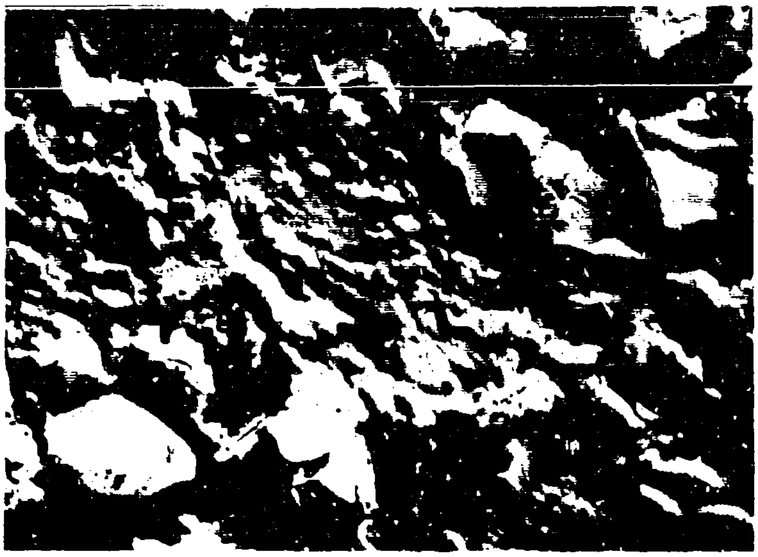

#65303 1500X

Figure 2.1 Structure of 500 Grit Diamond Ground MgO.

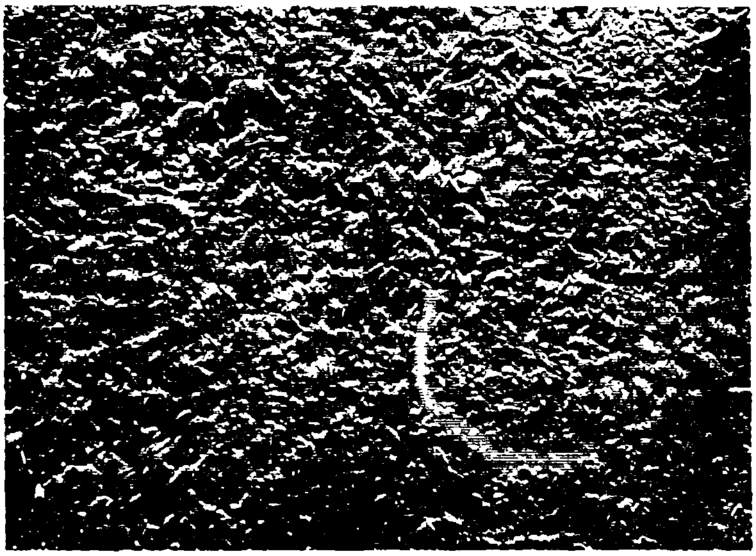

69692 7500X

Figure 2.2 Surface Structure of Chemically Polished Al_2O_3.

3. Sample and Test Arrangement

Transverse bend specimens were 0.100 inches high by 0.200 inches wide by 1.75 inches long, and on the edges of the tensile surface a 1/64 inch radius was honed.

The dead load tests were conducted in a lever arm test frame equipped with microswitch-clock arrangement to record time to failure. A brass 4-point bend test fixture was equipped for holding liquids, and tungsten (outer) and alumina (inner) knife edges were employed. The majority of the stress corrosion tests were conducted with the test specimen submerged in distilled H_2O.

The Al_2O_3 tests were conducted in four-point bending within a tungsten mesh, high temperature vacuum testing furnace* at a strain rate of 5×10^{-3}/min. Each specimen after placement on the test jig was given a vacuum (10^{-6} mm Hg) outgas at 900°C for 1 hour. This cycle was chosen in an attempt to desorb chemisorbed as well as physi-sorbed water and other possible corrosive surface contaminants, yet have the temperature sufficiently low to have minimum effect on microstructure. The specimen was allowed to furnace cool and tests were conducted at the temperature of the water coolant running on the outside of the furnace. Dry argon (at 1 atm.) was introduced into the test chamber without breaking the chamber to air and tests were conducted within several minutes of introducing the argon. This is believed to allow testing of specimens with a water-free surface in a nearly water-free environment. Control tests were conducted on samples given the same treatment except that air (relative humidity of 55% at 72°F) was introduced into the chamber and was the atmosphere during testing.

C. Magnesia

1. Results

The magnesia stress corrosion study was conducted with specimens machined from one billet having a density of 100%. A slight density gradient was noted in the billet with specimens varying between 100% dense and 99.6% dense. Care was taken to randomize the specimens so that testing at any one stress level was conducted with the full range of specimen densities. The 8 micron grain size intercept measured for the billet was quite uniform throughout.

The test results are listed in Table 2.1. The dead load tests were conducted at fractions of between .93 and .50 of the "dry" moderate strain rate average fracture stress. The stress corrosion behavior is illustrated in Figure 2.3.

Replica electron microscopic techniques were employed to study surface and fracture effects of MgO tested under water (H_2O) at constant stress levels of 22.8 kpsi and 12.1 kpsi. Specimens fractured in conventional "dry" test conditions were also examined for comparative purposes.

---

* Centorr Associates, Suncook, New Hampshire.

TABLE 2.1

DELAYED FRACTURE TEST ON MgO, TESTED IN H_2O

Specimen/Density*		Load, Kpsi	Time to Failure, sec
Mg-2-13	I	12.0	1.86×10^6
Mg-2-24	H	14.0	3.86×10^6
Mg-2-18	I	16.0	1.64×10^6
Mg-2-19	H	16.0	1.60×10^6
Mg-2-17	L	17.0	3.36×10^2
Mg-2-22	L	17.0	3.10×10^3
Mg-21-11	I	17.0	5.84×10^5
Mg-2-12	H	17.0	8.57×10^5
Mg-2-21	L	18.4	0.0
Mg-2-20	I	18.4	1.50×10^3
Mg-2-16	H	18.4	5.50×10^3
Mg-2-23	L	19.85	1.0×10^2
Mg-2-15	L	19.85	1.29×10^3
Mg-2-9	I	19.85	1.13×10^3
Mg-2-10	H	19.86	1.47×10^3
Mg-2-14	L	22.5	0.0
Mg-2-5	I**	22.5	2.34×10^2
Mg-2-6	H**	22.5	2.10×10^3
Mg-2-7	I	22.5	0.0
Mg-2-8	H	22.5	2.4×10^1

Six specimens 24.3± 3.0 Kpsi (2 from each group)	Tested in argon at $\epsilon = 8 \times 10^{-5}$ sec^{-1} after 900°C - 1 hour anneal

---

* H - density high 3.584 gm/cc - 0.0% porosity
I - intermediate density, 3.578 0.2% porosity
L - low density 3.570 gm/cc 0.4% porosity
** test in 55% air

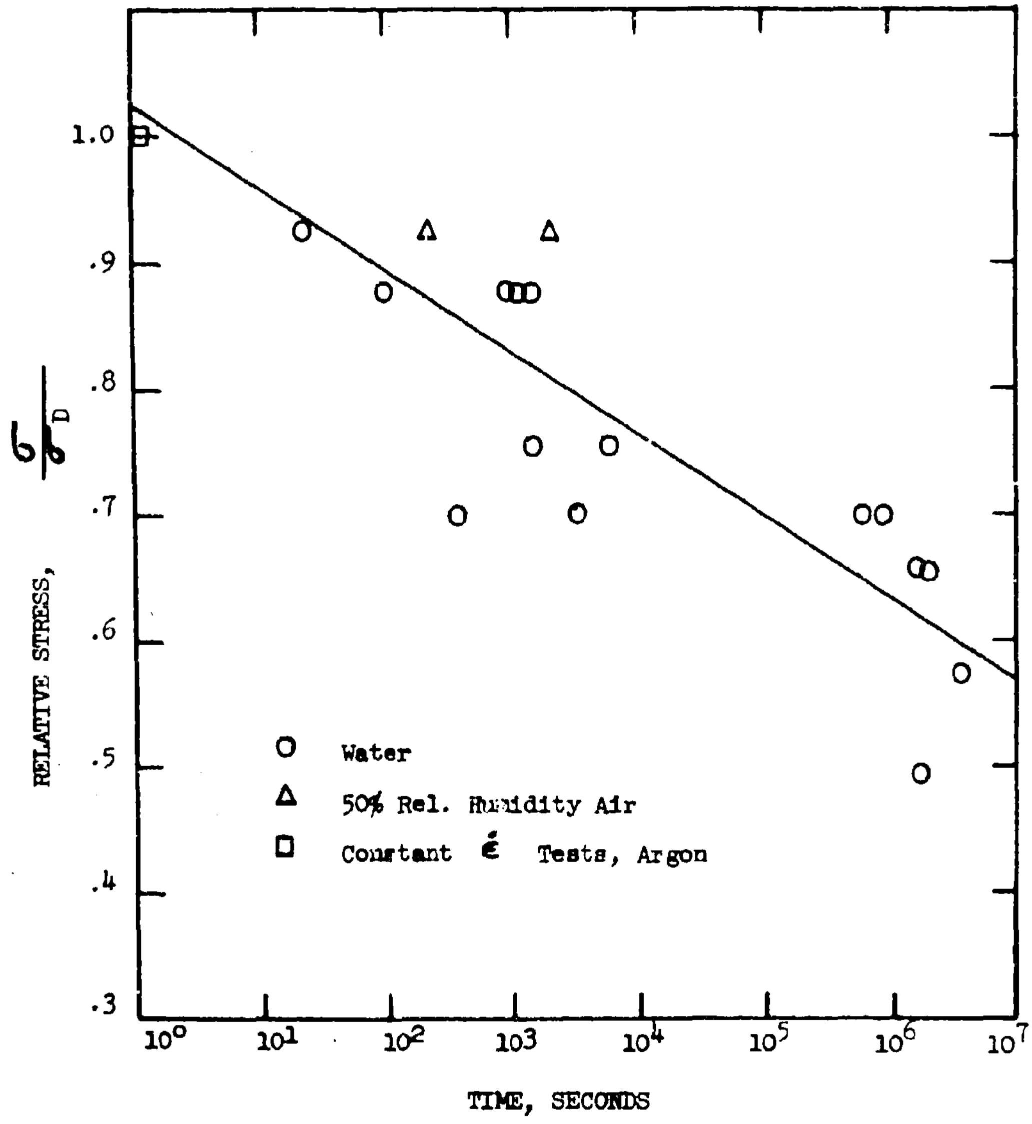

Figure 2.3

Relative Strength versus Time of Load Application for MgO Showing Detrimental Effect of Water.

The pressure sintered MgO used in the experiments fractured predominantly by intergranular mechanism as shown in Figure 2.4. A moderate amount of second phase impurities are present in the grain boundaries as illustrated in Figure 2.5. The powder used for pressure sintering this material contains Al, Ca, Na and Si as impurities which are known to segregate at the grain boundaries.[11] Since processes dependent on the grain boundary conditions such as stress corrosion could be greatly affected by these impurities, it is necessary to ascertain the extent and nature of the species located at the boundaries. Electron diffraction analysis of extracted particles near areas apparently containing high concentrations of the impurities (Figure 2.6) gave crystal patterns which could be indexed as sodium aluminum silicates (Table 2.2). The presence of these second phase compounds also tend to complicate interpretation of the fracture characteristics associated with corrosive type failure.

Intergranular fractures and secondary cracks at grain faces are commonly observed in stress corrosion and hydrogen embrittlement failures in metals.[12] Similar cracks were observed at the fractured grain faces (Figure 2.7) of MgO tested under water. Most of the specimens fractured in water also exhibited a corroded appearance at the grain boundaries (Figure 2.8).

2. Discussion

It is clear that the dead load tests illustrate a classic delayed failure curve. This result was entirely unexpected from the moderate strain rate (8 x 10^{-5} sec^{-1}) tests.

Charles[13] performed a cursory study of stress corrosion in single crystal MgO. He found evidence for stress corrosion at 240°C testing under compression in dry nitrogen and saturated water vapor. Similar tests at room temperature gave mixed behavior. Considering the known hydration behavior of MgO, they speculated that stress corrosion in the classic manner for glass had occurred.

In contrast, there is abundant information that dislocation motion plays a role in fracture at room temperature and above. Higher fracture stresses and decreased ductility have been observed when single crystal surfaces have been chemically polished,[14,15] which is thought to be a result of removing mobile dislocations normally introduced through handling damage. Similar results have been observed in bicrystals and high density polycrystalline magnesia.[15] Tensile strengths of over 100,000 psi were observed for fresh dislocation-free single crystals and bicrystals while a tensile strength of 35,000 psi was reported for polycrystalline material[15] with a similarly prepared surface. Clarke et al[8] have proposed a mechanism in which dislocations interact with pre-existing subcritical Griffith flaws and propagate the crack through the influence of the piled up dislocation strain field. This mechanism is a variation of a theory advanced by Cottrell.[16] Recently, Rice[17] examined fracture surfaces on extruded MgO having a pronounced (100) texture, and concluded that fracture was initiated from some point to 2 to 8 grains deep in the specimen by the intersection of slip bands and subsequent nucleation of a crack. More recently, Westwood et al[18] introduced dislocation half-loops on freshly cleaved MgO and studied the effect of adsorbed species on dislocation mobilities. He was principally interested in explaining the delayed creep

#69652 1500X

Figure 2.4 Electron Fractograph of Sintered MgO Showing Predominantly Intergranular Fracture.

#69654 7500X

Figure 2.5 Fractograph of Impurity Phase at MgO Grain Boundaries.

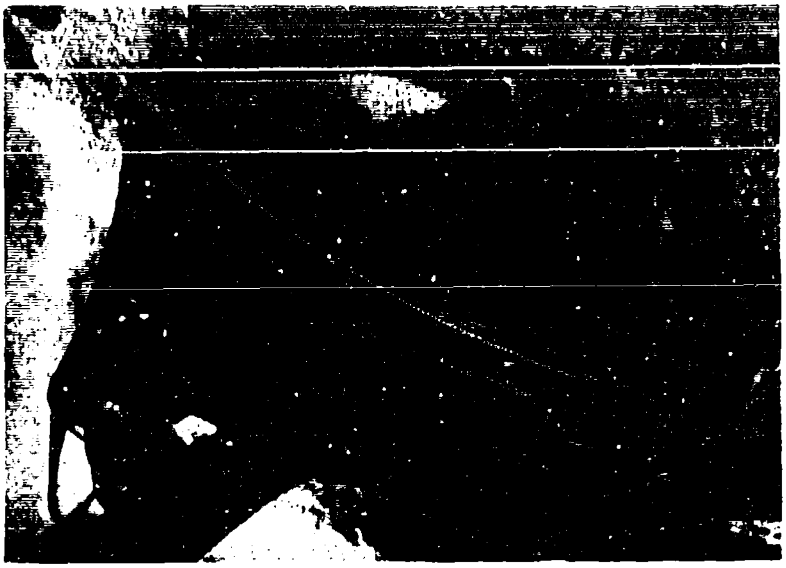

#69672 (a) 30,000X

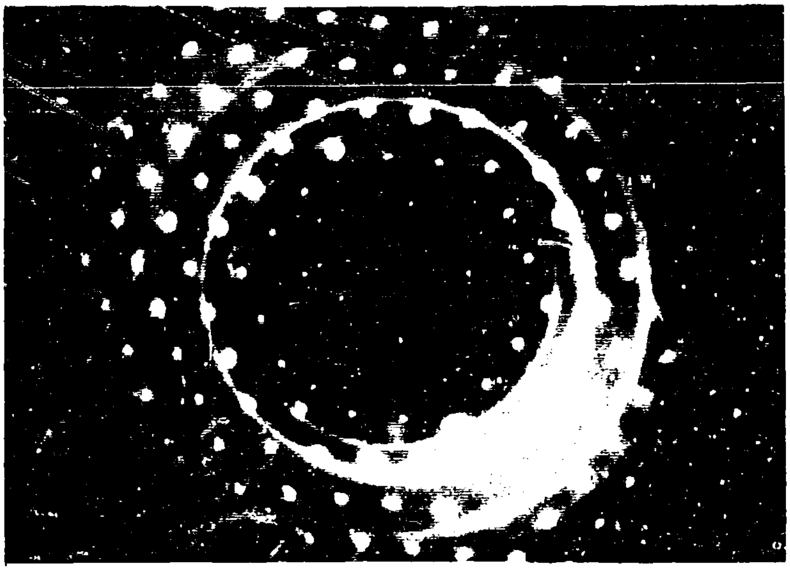

(b)

Figure 2.6 Electron Micrograph (a) and Associated Electron Diffraction Pattern (b) of Extracted Particles MgO Fracture Surface.

TABLE 2.2

ELECTRON DIFFRACTION DATA OF GRAIN BOUNDARY PHASE IN MgO

Measured dÅ Values	ASTM 10-31 $Na_6Al_4Si_4O_{17}$		
	dÅ	I/I1	hkl
4.23	4.21	80	111
2.54	2.58	100	220
2.12	2.10	3	222
1.66	1.82	10	400
	1.67	5	331
1.48	1.49	35	422
1.27	1.40	1	511, 333
	1.29	6	440
1.23	1.23	3	531

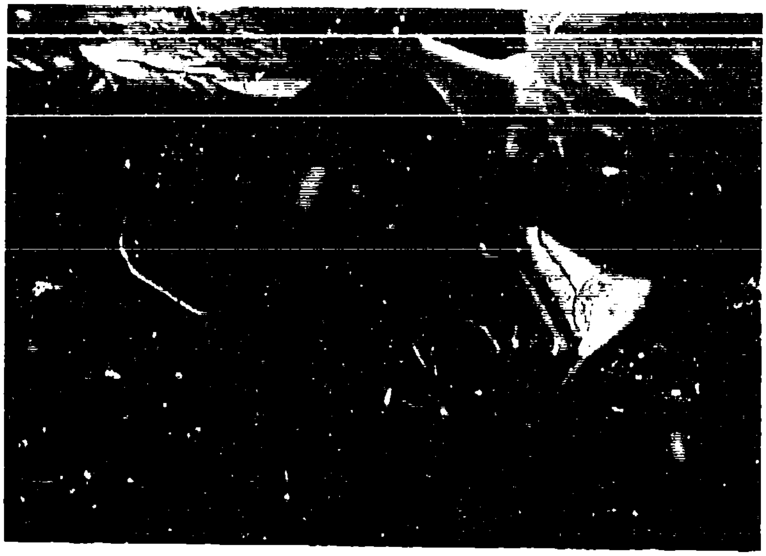

#69585 7500X

Figure 2.7 Secondary Cracks at Grain Faces of Stress-Corrosion Fractured MgO.

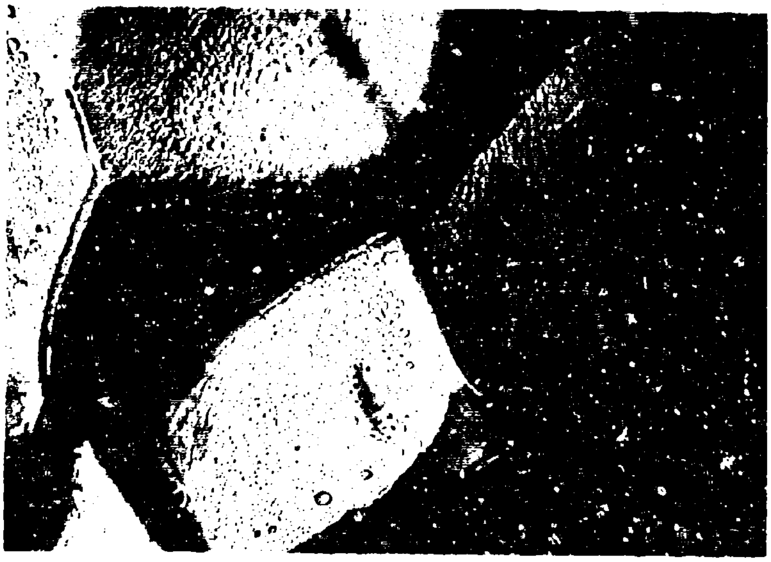

#69662 7500X

Figure 2.8 Corroded Appearance of Grain Faces and Boundaries in MgO.

phenomena found by Westbrook and Jorgenson.[19] Complexes of high positive or negative charge or molecules of high dipole moment significantly enhanced dislocation mobility giving what is termed a Rebinder effect. Thus, dislocation velocity is apparently influenced by environment and a mechanism for a delayed dislocation nucleated brittle fracture in MgO may be forwarded.

Assuming that the classic stress corrosion mechanism of Charles and Hillig[20] is operative, the stress corrosion curve may be used to calculate the activation volume, V^*. The model assumes that an element of material containing a semi-elliptical surface flaw is under a uniaxial stress. The kinetic process associated with the assumed chemical corrosion reaction at the crack radius is linearly related to hydrostatic pressure in a manner analogous to diffusion or ionic conductivity in solids. The activation volume is the proportionality constant for the pressure term. In the expression, velocity, V, of the corrosion reaction is

$$V = V_o \exp -\left[A - V^*\sigma + \gamma V_m/\rho\right] \qquad (1)$$

where V_o = a constant

A = an activation energy

γ = surface free energy between the solid and reaction product

V_m = molar volume of solid material

ρ = radius of curvature of interface

σ = the local stress

It can be shown[20] that the delayed failure curve related to this basic equation (1) by the relation

$$\ln (t/t_{0.5}) \approx -\frac{V^*}{RT} \sigma_{th}\left[\frac{S}{S_D} - \frac{1}{2}\right] - f\left(\frac{S}{S_D}\right) \qquad (2)$$

where t is the time-to-failure, $t_{0.5}$ is the time-to-failure at 1/2 of the "dry" strength, S_D: the term $-f\,(S/S_D)$ is a slowly varying function which relates the short time behavior of a fatigue system to the time behavior of the system as it approaches the fatigue limit.

The slope of the line in Figure 2.3 is -0.067 thus,

$$\frac{d \ln t}{d \ln (S/S_D)} \approx \frac{V^* \sigma_{th}}{RT} \approx -15\ (2.3) \qquad (3)$$

The modulus of elasticity, E, of MgO is 3.17×10^6 Kg/cm^2, and assuming that $\sigma_{th} \cong E/5$, the $\sigma_{th} \simeq 6.34 \times 10^5$ Kg/cm^2. The activation volume, V^*, or corrosion reaction resulting in the fatigue of MgO is about 1.37 cc/mole (referred to a uniaxial stress). Typical values found by other investigators are 0.5 cc/mole for carbon in Fe, 0.66 cc/mole for stress corrosion in Al_2O_3, and 4.0 cc/mole for alkali metal ion diffusion in silicate glasses.[21]

The second basic equation for this fatigue theory is as follows:

$$S_L = \left[\frac{3\ \sigma_{th}\ \gamma\ V_m}{8\ V^*\ L}\right]^{1/2} \qquad (4)$$

where S_L is the fatigue limit and L is the initial depth of the flaw.

The value of S_L was not found in this study, but an estimate of γ, the surface energy between the reaction product and MgO can be made by making two assumptions: 1) $S_L \approx 0.2\ S_D$ as was found for Al_2O_3[21] and 2) L is equal to the grain size or 12 microns for this MgO sample. The ratio of γ/L is approximately 6 x 10^4 ergs/cm^3, so for the 12 micron flaw, γ is 68 ergs/cm^2. This value appears low, but it is probably correct within an order of magnitude. A value of 20 ergs/cm^2 was obtained by Charles and Shaw for alumina.[13] Thus, the MgO data is readily treated by standard stress corrosion models, and results in readily comparable values for the activation volume and surface energy between MgO and the corrosion product.

In view of the evidence for dislocation nucleated fracture in MgO the possibility of stress corrosion by a mechanical model analogous to those invoked for metals should be considered. The brittle film model for example, involves the formation of a corrosion product film which fractures after a certain time due to the elastic stress concentration. The crack propagates into the matrix for a short distance only to be halted by plastic flow. This process continues until either the flaw becomes so deep that the specimen fails or dislocations from this discontinuous crack propagation pile-up on a grain boundary and nucleate fracture when the back stress becomes too high. The secondary crack on the fracture surface (Figure 2.7) may be evidence for this phenomenon.

It is not possible to decide between a mechanical and classic chemical stress corrosion model at the present time. The lack of stress corrosion behavior at moderate $\dot{\epsilon}$'s leads to the conclusion that a reaction is involved with kinetics requiring somewhat over a minute to become effective. It should be mentioned again that evidence for a minor sodium aluminum silicate grain boundary phase was found. Thus, the possibility exists that the corrosion response is that of the grain boundary phase and is not an intrinsic property of MgO. This comment, of course, can be made about most of the property work on MgO to date, and is certainly an argument for the generation of high purity MgO samples (Section III).

D. Alumina

1. Results

Specimens were machined from one billet, C33, which possessed a grain size of 2 microns and a density of 99.8%.

The results for the tests conducted according to the procedure outlined are given in Table 2.3. There was no apparent strengthening due to the chemical polishing. The two groups of polished samples did have a higher standard deviation in strength than the unpolished samples which was a result of bend strengths as high as 75.4 Kpsi and as low as 44 Kpsi.

2. Discussion

The Al_2O_3 tests failed to confirm the previous finding that stress corrosion limits the bend strength at moderate strain rates to ~ 0.8 of the "dry" strength. The above tests were conducted on Al_2O_3 + 1/4% MgO rather than pure Al_2O_3 as previously tested. Charles and Shaw[21] tested Lucalox (Al_2O_3 + 1/4% MgO), and found evidence for stress corrosion. Therefore, it would appear that the MgO addition per se is not responsible for the lack of collaboration.

The question must be raised, however, whether the MgO assumes an identical distribution and form when hot pressed as compared with the sintered product. The temperatures and times are both lower and shorter for hot pressing thus conditions are less favorable for complete solution. Another point for consideration is that MgO itself did not exhibit a stress corrosion response when tested in an identical manner to that above.[3] It is suggested, therefore, that the form of MgO in hot pressed Al_2O_3 may be responsible for the lack of stress corrosion behavior in the above tests. This suggestion, however, implies a great deal concerning the strength behavior of such a body, and the authors are not prepared to delve into all of these questions with the limited data available.

There is also the possibility that some experimental problem, e.g., wet argon, failure to load specimen uniformly, etc., was the cause of the above behavior.

With the overwhelming evidence from the previous studies,[3,21] the authors still believe that stress corrosion plays an important role in room temperature failure of Al_2O_3.

The testing was rather inconclusive concerning the effect of the chemically polished surface structure on 23°C bend strength. From the high strengths obtained on several specimens it appears that chemical polishing is at least capable of reducing flaw lengths and increasing strength. However, to accomplish this for an entire gage length of a specimen is an improbable proposition.

The previous conclusion that an air anneal is the most effective means of reducing flaw size and density in Al_2O_3 still holds. However, in view of the recent discussion by Rice[35] of gaseous impurities in hot pressed bodies the above conclusion should be tested in a more conclusive manner.*

III. CHARACTERIZATION AND DENSIFICATION OF HIGH PURITY ALUMINA AND MAGNESIA

A. General

---

* Similar to the tests conducted by the authors[3] on MgO where $\sim$ 100 micron layer is ground from control samples given on identical heat treatment to those being tested as "heat treated".

Table 2.3

Chemical Polishing Experiment on Al_2O_3

Surface Condition	Test Atmosphere	Sample Mean Fracture Strength kpsi	Standard Deviation kpsi	Number of Samples
500 Grit Diamond Machine	Air-no heat T	50.0	7.8	5
	Air-no heat T*	56.0	8.0	5
Mech. Pol - then Chem. Polished	Air-heat T	57.3	8.4	6
	Argon-heat T	50.0	9.6	6
As ground - then Chem. Polished	Argon-heat T	60.1		1

* Heat Treatment - Consisted of heating to $900^{\circ}C$ for 1 hour in vacuum the furnace cooling

There is general agreement that property measurements on single and polycrystalline ceramics have to date reflected extrinsic behavior. Furthermore, the lack of sufficiently pure specimens has made it difficult, if not impossible, to unequivocably separate structure-sensitive from composition-sensitive properties. Properties sensitive to point defects such as electrical conductivity, diffusion and hardness are thought to be particularly sensitive to composition. For example, Aust and Westbrook[22] have found that grain boundary hardening is associated with impurity-vacancy interactions. There is considerable evidence that grain growth rates are impurity sensitive. Also, line defects and their response to imposed stress are known to be dependent on impurities. These facts lead one to anticipate an effect of chemical purity on the mechanical properties of oxides.

Much of the mechanical property work by the authors and others[1,2,3,17] to date has been based on materials made from Linde A Al_2O_3 (99.9%) or Fisher Electronic Grade MgO (99.4%). Leipold[11] has shown that MgO of this purity develops visible grain boundary precipitates when heated to approximately 2200°C and that segregation undoubtedly is present in hot pressed material (see Section II). It is reasonable to predict that some of the mechanical properties of MgO will depend on this impurity segregation. Although evidence for impurity segregation or precipitation is less conclusive for Al_2O_3, it is assumed that similar effects will be found. The question of gaseous impurities, particularly on hot pressed material, is extremely important, and must be considered in an analysis of impurity effects.

Preliminary lots of Al_2O_3 and MgO were evaluated in a previous program.[1] Several possible sources of Al_2O_3 were found and the fabrication behavior was studied. All but one source of Al_2O_3 was eliminated from consideration because the agglomerate structure resulted in an inhomogeneous porosity distribution and exaggerated grain growth was prominent perhaps because of an inhomogeneous impurity distribution. The high purity MgO obtained was too coarse in particle size for adequate densification, so it was decided to produce MgO with a controlled particle size by calcining high purity $Mg(OH)_2$ as fine powders can be produced in this manner.[23] A great deal of difficulty was encountered in producing dense samples containing a uniform grain size.

The goals for the program to be described in the following section were to fabricate, with minimum contamination, high density MgO and Al_2O_3, to characterize the fabricated samples and to make property measurements for comparison with data for the "standard" grades of Al_2O_3 and MgO.

B. Results and Discussion

1. Chemical Characterization

The powders used for this program and the reported purity are listed in Table 3.1.

TABLE 3.1

SOURCES OF HIGH PURITY POWDERS

Material	Supplier	Lot No. or Grade	Suppliers Reported Cation Purity
Al_2O_3	United Minerals Dist. of Johnson-Matthey, New York	S.1 S.3109 S.5578	99.9995

TABLE 3.1 (Concl'd)

SOURCES OF HIGH PURITY POWDERS

Material	Supplier	Lot No. or Grade	Suppliers Reported Cation Purity
$Mg(OH)_2$	United Minerals Dist. of	SH194	99.9989
	Johnson-Matthey, New York	SH182	99.9954

a. Chemical

Three analytical tools were utilized in the chemical analysis of the powders; namely, emission spectroscopy, plasma source mass spectroscopy,* and spark source mass spectroscopy.** Emission spectroscopy is a well known analytical technique for determining cation impurity concentrations with a typical detection limit of from 1-10 ppm.

Plasma source mass spectroscopy is less common, but it offers great sensitivity, flexibility and mass coverage. The spectrograph utilizes a plasma of 5-6 KV potential which is low enough that the ionization potential of each impurity becomes important. It is, therefore, necessary to determine sputter ion yields to generate quantitative data. These are difficult to obtain as they are matrix sensitive. Very good qualitative and comparative data can be obtained without determining sputter ion yields, however, by estimating these yields based on experience with similar matrices. The plasma can be directed at a spot on an outer or fractured surface of a specimen, and sputtering can be continued until an internal fresh area is analyzed. This feature of the analysis is a distinct advantage over the spark source, which requires dilution of the sample, and subsequent handling by incorporation into a high purity carbon or silver electrode. However, the plasma analysis is selective due to the limited area of the beam and an area not representative of the entire body may by chance be analyzed.

The spark-source mass spectrograph utilizes an RF spark operating at 50-60 KV potential and hence the ionization potential of individual ions does not enter the calculations - all ions are ionized. However, this introduces some complexity in the analysis as a multiplicity of charged ions per element often occurs. On the other hand, this multiple ionization is advantageous for species which have high thermal-ionization efficiencies as local heating of the electrodes in the spark area is unavoidable; therefore, it is assumed that the first stage of ionization for such ions as Na^{1+} and K^{1+} comes in part from the electrodes and is not representative of the sample. In this case, the analysis is conducted on the Na^{+2} or K^{+2} peaks. The spark source analyses a larger volume element of the material than the plasma source, thus it may give a better average analysis. The reproducibility for both spectrographs is of the order ± 50%; however, accuracy is usually quoted to be of the order of a factor of three.

The analyses for Al_2O_3 powder from the above source and several fabricated samples are listed in Table 3.2. The agreement among the three

---

* Performed by Dr. Frank Satkiewicz, GCA Corporation, Bedford, Mass.

** Performed by D.C. Walters and E.R. Blosser, Battelle Memorial Institute, Columbus, Ohio.

TABLE 3.2

ANALYSIS OF HIGH PURITY* Al_2O_3 POWDER

AND FABRICATED SAMPLES

Impurity Element	No. 1 Powder	Plamsa Source Mass Spec. No. 2 Powder ppmw	Plamsa Source Mass Spec. No. 1329 Sample	Yield(2) Factor	Spark Source Mass. Spec. Sample 1331 ppmw	No. 1 Powder ppmw	Emission Spec. No. 2 Powder	Emission Spec. Sample No. 1188
H	0.004(1)	0.2	0.02	5(1)	NR			
B	2.1	3.2	3.2	0.01(0.1)		1	1	2.5
Be		1.1	0.8		2	ND		
C	4.7	ND	17.6	0.01(0.1)	NR		10	160
N	2.7			0.01(0.1)	NR			
F	3.7	2.8	389.	0.01(0.1)	6		7	1
Na	0.02	13.6	5.6	5(50)	40	1	1	1
Mg	0.6	.5	4.8	1(10)	100	1-5	16	16
Si	9.1(3)	4.1	11.0	0.3(1)	50	1-5	3	3
P	9.1	7.6	3.0	0.01(0.1)	1			
Cl	10.7	6.9	6.9	0.01(0.1)	40			
K	1.2	22.9	15.3	5(50)	30	1-5	1	1
Li		0.5	0.1		0.3	1		
Ca				1(10)	30	5	14	14
Ti	0.1	1.9	0.4	2(10)	0.6	1-5		
Cr	0.4	0.3	0.5	0.5(1)	3	ND		
V	1.0	0.4	3.0	0.2(1)	0.1			
Mn	0.4	0.3	1.6	0.5	1	1	1	1
Fe	1.1	-	76.7	0.2(1)	20	1	1	1
Cu	25.9			0.5(0.6)	0.5	1-5	1	1
Zn					6.0	ND	1	1
Ga					1.0	1		
Y					0.1	ND		
In					0.1	ND		

TABLE 3.2 (Concl'd)

ANALYSIS OF HIGH PURITY* Al_2O_3 POWDER AND FABRICATED SAMPLES

Impurity Element	No. 1 Powder	Plasma Source Mass Spec. No. 2 Powder ppmw	Plasma Source Mass Spec. No. 1329 Sample	Yield$^{(2)}$ Factor	Spark Source Mass Spec. Sample 1331 ppmw	No. 1 Powder ppmw	Emission Spec. No. 2 Powder	Sample No. 1183
Pb					0.2	ND	1	1
S					10		25	110.
Ni		4.3	11.5		1			
Ga					1			
Sr					1			
Zr					1			
Rb		0.2	0.2		3			
Sb					1			
Cs		0,3	0.3		3			

* Johnson Matthey Lot S5578

(1) poor baseline

(2) yield factors in parentheses are for analysis reported in April 1967 Summary Report

(3) analysis for Si based on atomic spectra to avoid AlH+

Mass spec. = plasma source molecular spectra

$$\text{ppmw} = \text{ppma} \frac{(\text{m.w. of element})}{(\text{m.w. of } Al_2O_3)}$$

techniques varies between being quite good (with a factor of two) to quite poor $\sim$ a factor of 5. Under these conditions, it is difficult to know which analysis to believe for an absolute determination of concentration. It must also be borne in mind that accidental contamination prior to analysis could influence one or more of the analyses. Fabricated samples Nos. 1329 and 1331 were given a 50°/hr to 1200°C - 16 hour air anneal prior to analysis (wrapped in Pt foil) whereas 1188 was analyzed as "hot pressed". It is interesting to note that the emission spectroscopy analysis of Sample 1188 revealed a 150 ppm pick up of carbon whereas the annealed samples were substantially lower. Sulphur contamination also occurs during hot pressing and it is thought that the source for sulphur is the graphite hot pressing die. The plasma source analysis showed an abnormally high F content which was not detected in the original analysis (No. 1) or by the other techniques. It was also found in the MgO analysis conducted at the same time. So, there is some question whether this is actually present in the sample or the result of either machine or sample contamination from an outside source not connected with the fabrication effort.

The analyses for MgO produced from the two J-M lots of $Mg(OH)_2$ and several fabricated samples are listed in Table 3.3. The absolute agreement in impurity concentration was not good particularly for Fe, K, Al and F. Na was clearly the most important powder impurity, but it appeared to have been driven out during either hot pressing or the slow 1200°C air anneal (same conditions as for Al_2O_3). According to the spark source analysis, the most serious impurities for MgO (tranditionally Si, Ca and Fe) are present at moderate levels both in the powder and fabrication samples.

Several years ago, M. Leipold conducted a program to synthesize and fabricate high purity MgO. A program was conducted at Battelle to develop analytical techniques to augment the synthesis effort. E.R. Blosser of Battelle was the principal investigator on the analytical program.[24] As the spark source mass spectrographic analysis reported in Table 3.3 was conducted under his direction, presumably on the same spectrograph, it was of interest to compare the analysis of the Avco sample with several fabricated under the direction of M. Leipold. Table 3.4 shows just the major impurities (excluding H) for both types of samples. It appears that in general, the Avco material is lower in S, Cl and Ti and the JPL material is lower in Na, Si and Ca while Fe and Zn are about equivalent. On a total impurity basis JPL 63 was clearly the purest with Avco 1330 ranking second. Si and Ca are extremely bad impurities in terms of segregation and second phase production thus, the JPL samples are more likely to be free of such effects.

The physical characteristics of the two powders employed were fully discussed.[3] To summarize briefly, S5578 Al_2O_3 is 58 v/o α Al_2O_3 with the remaining transitional (mostly γ Al_2O_3) phases. the mean size of α is 1500 A° and the mean size of γ is 240 A°, and the surface area is 24.4 m^2/gm. The calcined MgO exists as 20-50 A° size particles within a loosely bonded 0.1 to 0.5 microns agglomerate which is apparently a relic of the $Mg(OH)_2$ platelet. X-ray techniques demonstrated that some $Mg(OH)_2$ remains after the 350°C - 1 hour calcine.

2. Consolidation and Structure

Considerable care was taken in die cleaning and powder transfer operations. All loading operations were conducted within a glove box. The precautions to prevent contamination have been described in detail previously.[3]

TABLE 3.3

ANALYSIS OF HIGH PURITY* MgO POWDER AND FABRICATED SAMPLES

Element	Plasma Source Mass Spectroscopy Sample No. 1328 ppmw	Spark Source Mass Spectroscopy Powder SH 182	Spark Source Mass Spectroscopy Sample No. #1330	Emission Spectroscopy Powder SH 194
Li	2.6	2.	2.	
Be		< 0.02	< 0.02	
B	8.1	0.5	0.5	10
F	329.	≤ 10.	≤ 10.	
Na	6.8	1500.	40.	
Mg		--	--	
Al	101.	4.	4.	10-100
Si	146.	150.	150.	10
P		1.	1.	
S		130.	10.	
Cl	237.	10.	3.	
K	0.234	20.	5.	
Ca	< 179	100.	100.	< 10
Sc		< 0.1	< 0.1	
Ti		≤ 1.	≤ 1.	< 10
V		0.1	0.4	10
Cr		0.2	0.4	ND
Mn	17.6	1.	1.	< 10
Fe	526.	4.	20.	10
Co		0.4	0.4	
Ni	19.	0.4	4.	
Cu		5.	3.	< 10
Zn		≤ 3.	20.	ND
Ga		< 0.4	< 0.4	
Sr		< 1.	< 1.	
Y		< 0.2	< 0.2	
Zr		< 0.1	< 0.4	
Nb		< 0.2	1.	
Sn		< 0.4	1.	
Te		1.	< 0.2	
Pb		4.	0.6	
H	1.49			

Johnson Matthey lots SH 182, SH 194 ($Mg(OH)_2$

TABLE 3.4

COMPARISON OF SPARK SOURCE MASS SPECTROGRAPHIC ANALYSES CONDUCTED ON MgO FROM TWO HIGH PURITY PROGRAMS

	AVCO	Jet Propulsion Lab Sample No.*		
Element	No. 1330 ppmw	49 ppmw	56 ppmw	63 ppmw
Na	40	16	0.5	1
Si	150	160	58	5
S	10	330	83	16
Ca	100	50	33	50
Fe	20	50	20	5
Zn	20	33	8	8
Cl	3	660	330	66
Ti	<1	66	25	<16
TOTAL	344	1365	557	167

* E.R. Blosser, "Development of Chemical Analysis Techniques for Advanced Materials," JPL Contract No. 951578 (1968), p. 55.

The Poco graphite dies were outgassed at 1700°C for 1/2 hour prior to use.

Table 3.5 lists the hot pressing results for J-M alumina. As noted, little difficulty was experienced in obtaining high density. Of course, the choice of hot pressing conditions was based on prior experience with this grade of Al_2O_3 as well as experience with other grades of powder. Essentially, all of the runs were fully dense as indicated by the density and the high degree of translucency. The first three runs were also characterized by a macroscopically visible cloud of porosity dispersed throughout the specimens. It was thought that these were relics of the powder agglomerate structure that had failed to completely break down under the applied load during hot pressing. The discussion on microstructure which will reveal that exaggerated grain growth occurs very easily in this material. Thus, porosity entrapment leading to the observed "clouds" might readily occur. Sample 1329 was fabricated from powder that had first been screened through a 100 mesh nylon screen. This completely eliminated the macroscopically visible "clouds". Thus, this procedure was adopted as standard practice. A number of samples were fabricated in 1" diameter by 3/16" thick so mechanical property measurements could be conducted.

Microstructural examination of samples fabricated either for a short time (6 min.) at high temperature (1450°C), Figure 3.1, or for a long time (60 min.) at low temperature (1380-1400°C), Figure 3.2, revealed a marked tendency for exaggerated grain growth. The grain size was not large (average intercept; 2.0 μ for 1307 and 1.2 μ for 1325) but the ratio of grain sizes did lead to the above conclusion. It was thought that the apparent ease for exaggerated grain growth was related to both the high purity and the inhomogeneous distribution of the impurities present in the system. It was shown previously,[3] that impurities were not homogeneous in hot pressed samples or even in Vernueil grown sapphire rods. Thus, it is thought that in an impure sample, a sufficient concentration of impurities are present to stabilize normal grain growth. The high purity Al_2O_3 on the other hand contains local exceptionally clean regions which are capable of rapid grain boundary mobility. These areas act as centers for exaggerated growth.

Samples 1339-41 were fabricated under the same temperature-pressure conditions, but the hold time was reduced by 2/3 to minimize the grain growth. Figure 3.3 reveals that the tendency for exaggerated grain growth was still present, but the total growth experienced was somewhat less than for the 60-minute samples. The average grain intercept was 0.8 microns. Samples of both types have been included in the properties program.

Table 3.6 lists the hot pressing results for MgO. In contrast to the Al_2O_3 effort, a great deal of difficulty was experienced in the MgO fabrication effort. The microstructural goal was a uniform 10 micron grain size and density $> 99.4\%$ of theoretical (3.581 gm/cc). A number of specimens were fabricated with the desired density (3.560 gm/cc), but none of these possessed the desired small grain size.

A very unusual microstructure feature was encountered with great regularity while attempting to achieve small grain sizes by lowering the hot pressing temperature. Figure 3.4 illustrates this structure which appears to consist of regions of dense well-bonded grains and extremely fine ($\sim$1 micron) grains located both in patches and along grain boundaries. The origin of this

TABLE 3.5

HOT PRESSING CONDITIONS AND RESULTS FOR HIGH PURITY Al_2O_3

Run No.	Temp. °C	Pressure Kpsi	Time min.	Density gm/cc	Grain Intercept microns
1307	1450	15	6	3.986	2.6
1308	1480	15	60	3.988	
1325	1400	15	60	3.990	3.2
1326*	1400	15	60		
1329	1400	15	60	-	
1331*	1380	15	67	3.989	
1337*	1400	15	60	3.990	
1339*	1400	15	20	3.986	0.8
1340*	1400	15	20	-	
1341*	1400	15	20	3.993	

*1" diameter - all others 1/2" diameter

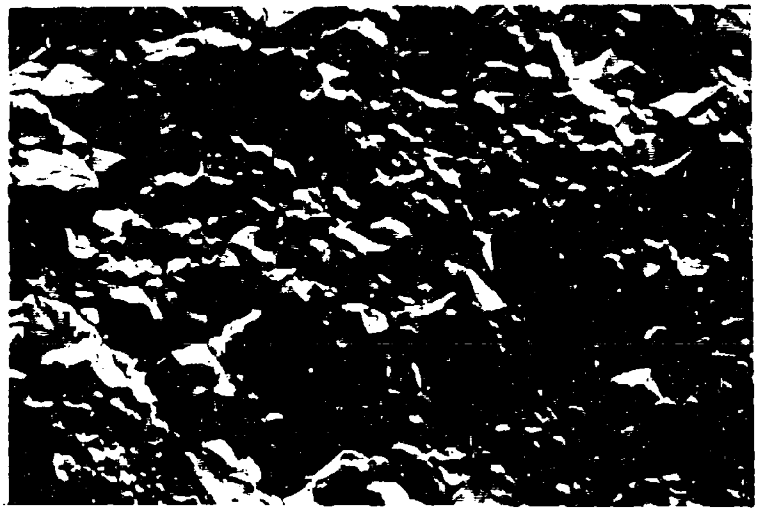

#69029 1500X

Figure 3.1 Electron Fractograph of Sample of 1307 Showing Some Evidence for Exaggerated Grain Growth.

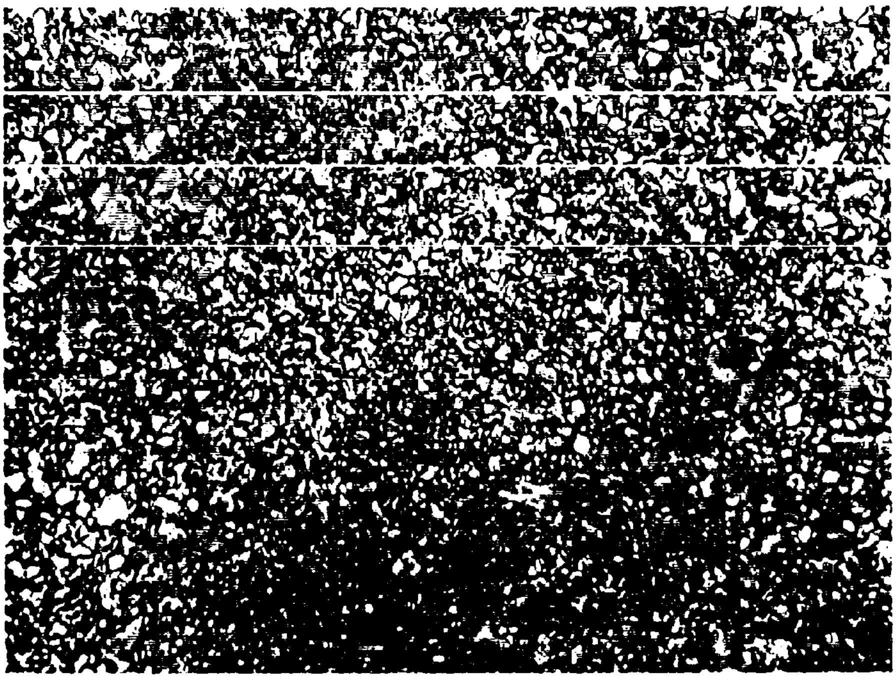

#5000-2 (a) 500X

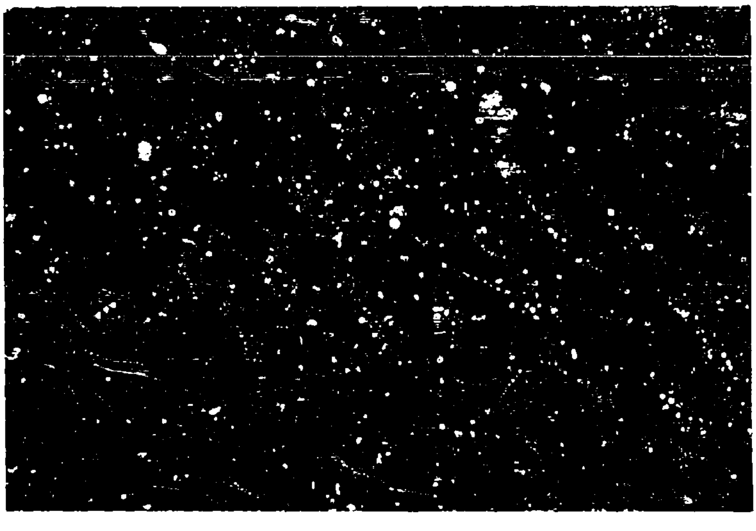

#69392 (b) 7500X

Figure 3.2 Optical (a) and Electron Replica of Polished and Etched Sample Exhibiting Some Evidence for Exaggerated Grain Growth.

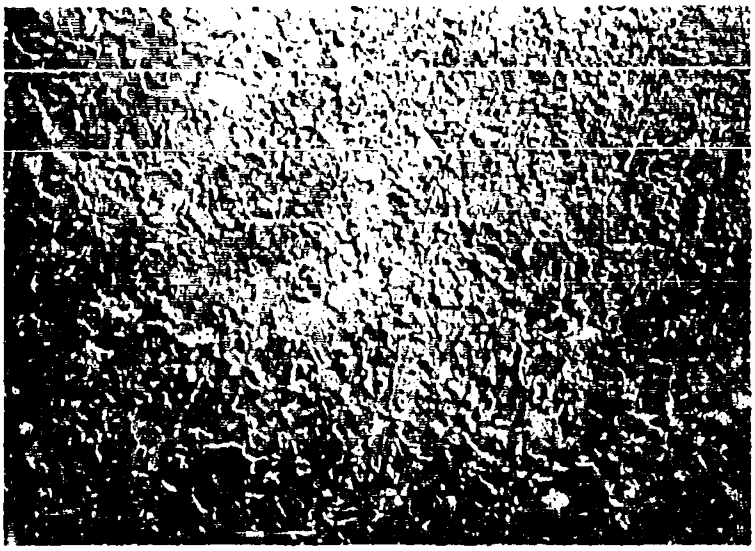

#69601 (a) 1500X

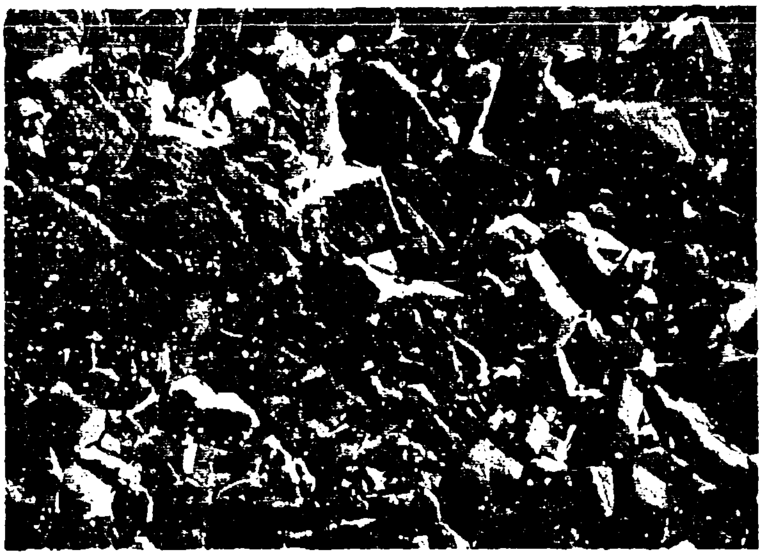

#69603 (b) 7500X

Figure 3.3 Electron Replica of Polished and Etched Sample 1339 Exhibiting Tendency for Exaggerated Grain Growth.

TABLE 3.6

HOT PRESSING CONDITIONS AND RESULTS

FOR HIGH PURITY MgO

Run No.	Temp. °C	Pressure Kpsi	Time min.	Density gm/cc	Grain Intercept microns
1299	1350	6	105	3.528	
1302	1300	15	90	3.562	18
1304	1350	10	48	3.561	20
1306	1400	8	90	3.535	
1309	1280	15	90	3.557	17
1310	1230	15	110	3.580	12
1311	1250	15	60	3.569	12
1314	1250	10	90	2.952	
1317	1150	15	105	3.597	
1319	1200	8	115	3.477	
1327*	1150	15	90	3.563	18
1328	1150	15	90	-	
1330*	1150	15	90	3.558	
1332*	1150	15	90	3.569	22
1342*	1150	15	90	3.570	
1343*	1150	15	90	3.563	

* 1" diameter - all others 1/2" diameter

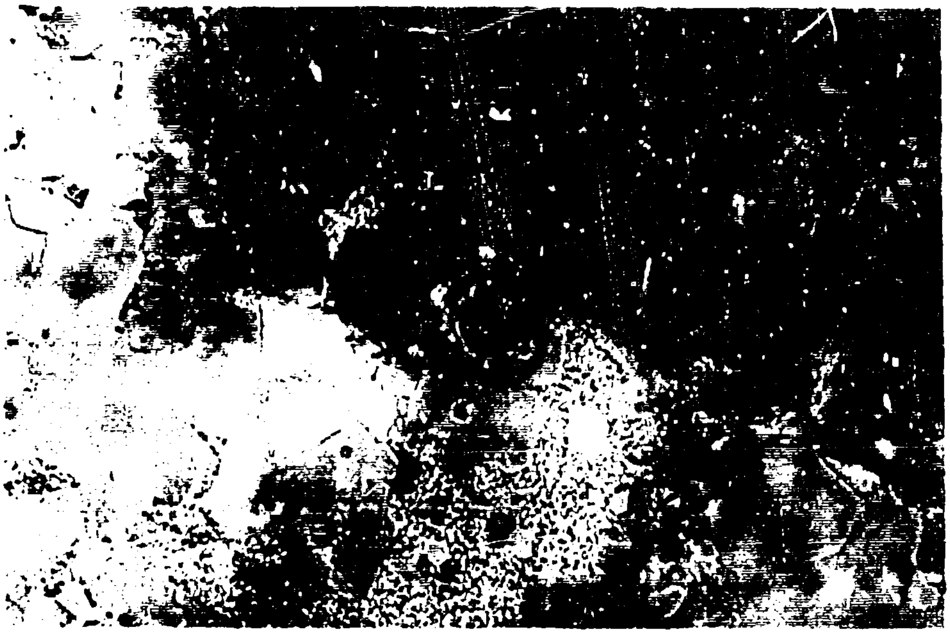

#5000-1 500X

Figure 3.4 High Purity MgO (Sample 1327) Hot Pressed at 1150°C Exhibiting Duplex Grain Size.

structure is not known, but it appears to correlate with the amount of $Mg(OH)_2$ remaining after calcination.

More uniform grain structures were obtained by hot pressing in the temperature range $\geq 1250^{\circ}C$ (Figure 3.5). The grain size is not as uniform as that obtained for less pure MgO, but the contrast with Figure 3.4 is marked. Grain growth studies (see Section III B 3) were conducted on samples 1241, 1243, and 1244 which had been hot pressed at 1400°C, and although the grain intercept is large ($> 35\ \mu$) the structure exhibits a more normal grain size distribution.

Thus, it appears that either due to residual $Mg(OH)_2$ or perhaps the impurity distribution model proposed for Al_2O_3, the high purity MgO fabricated in this program exhibited a duplex grain structure when fabricated at low temperatures (1150°C). Higher temperature cycles resulted in the disappearance of the fine grains presumably through the classic grain growth process. This grain growth process probably leveled the impurity concentration-distance curve which may have played an important role in the evolution to a nearly normal grain size distribution.

3. Properties

a. Mechanical Properties of Al_2O_3

Specimens 0.05" x 0.15" x 0.875" were machined from the 1" diameter Al_2O_3 specimens. Only 2-3 specimens were machined from each billet so to obtained a statistically significant number of tests at any one temperature required using samples from different billets. Tests were performed in two new pieces of apparatus designed to perform four-point bend tests on the above size specimen. The elevated temperature testing atmosphere was argon for all of the test results in this section.

The bend test results are given in Table 3.7. Also listed in this table are comparative data for hot pressed Al_2O_3 fabricated from Linde A powder. The "23°C dry" tests were performed by first heating the bar to 900°C for 1 hour in argon and then cooling to 23°C for the testing cycle without breaking the argon atmosphere. Similar tests were reported in Section II B, and previously except that a vacuum was employed during the heat treatment. The "23°C wet" test employed 55% relative humidity air.

The low temperature fracture strengths for the high purity samples were approximately equal to the reference values. The reference values chosen were the highest comparable strengths availab,e thus the comparison is thought to be critical but valid. It is noteworthy that a 20-30% strength drop was found going from "dry" to "wet" test conditions which correlates well with the stress corrosion phenomenon previously (Section II and ref. 3) discussed.

The high temperature strength values again appear to be as good, but the higher purity does not significantly alter the failure properties. Such might have been expected if, for example, intergranular bonding was improved due to decreased impurity concentration. From the chemical analyses of the hot pressed product, it is not possible to conclude that grain boundaries would be free of impurities.

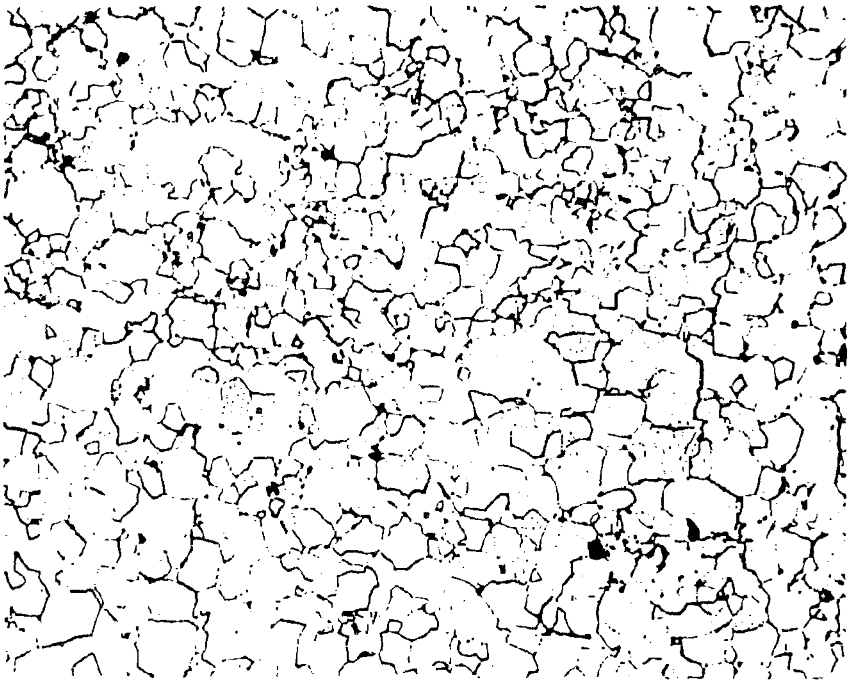

#4984-1 250X

Figure 3.5 High Purity MgO (Sample 1311) Hot Pressed at 1250°C Exhibiting Structure Close to Normal.

TABLE 3.7

BEND STRENGTH OF HIGH PURITY Al_2O_3

AND COMPARATIVE DATA

Sample Number	Bend Strength, Kpsi at				
	23°C wet	23°C dry	1200°C	1400°C at $\dot{\epsilon}$, 10^{-5} sec	1450°C at $\dot{\epsilon}$, 10^{-5} sec
1326	61.7	101.4	41.7		
1331	65.6	97.9 91.5			
1337		82.4	40.5 52.0		
1339					
1340					
1341				34.7/2.7	29.5/6.8
Reference Data					
FLU-2-Al_2O_3 + 1/4% MgO 1.3 u G.S.(1)	74 ± 10			35.7/43 35.9/5.8	
BR-1-L-Al_2O_3(4) 1.6 μ G.S.	72 ± 12	102 ± 11			
Reference (28) 2.2 μ G.S.			49		26
Reference (29) 1-2 μ G.S.				31	26

High temperature deformation studies were also initiated on 0.875" long specimens of high purity Al_2O_3. The tests again were four-point bend tests conducted in argon. Hafnium diboride knife edges contacted the sample. A W probe transferred the specimen deformation to an LVDT, and both strain and load versus time were recorded.

For brittle fracture tests, the procedure is straightforward using elastic theory to reduce load-deflection curves to fracture stresses and elastic moduli. For high temperature tests, a more complicated procedure is necessary in order to analyze the plastic flow which occurs. This results because the flow stress is, in general, a function of both strain and strain rate, and is not necessarily linear through the beam, thus invalidating the elastic stress analysis. When the stress is independent of strain and is linearly proportional to the strain rate, as in diffusional creep, the stress distribution is linear in the beam and the elastic equation may be used.[25]

Previous investigation in this laboratory has shown that the rate sensitivity, m, (from the empirical relation $\sigma = K\dot{\epsilon}^{m}$) is less than unity for fine grained alumina.[26] A procedure has been developed for determining the stress-strain-strain rate relations for materials which strain harden and are rate sensitive.[27] This requires the measurement of the bending moment as a function of deflection and deflection rate and the determination of the outer fiber stress from the relation:

$$\sigma = \frac{2\,m}{bh^2}\left[2 + n_b + m_b\right] \qquad (1)$$

where

$$n_b = \left(\frac{\partial \ln M}{\partial \ln \phi}\right)_{\dot{\phi}} \qquad (2)$$

$$m_b = \left(\frac{\partial \ln M}{\partial \ln \dot{\phi}}\right)_{\phi} \qquad (3)$$

where M is the bending moment, ϕ the angle of inclination of the neutral axis of the beam (proportional to the deflection), $\dot{\phi}$ the rate of change of ϕ , and b and h are the width and depth of the beam. The strain and strain rate are determined directly from the deflection by geometrical considerations. During a test the load and the deflection are continuously recorded versus time and the "outer fiber" stress-strain, and strain rate are calculated from this data. In general, a series of constant rate bend tests are made from which the desired relations are calculated. In the case of fine grained alumina the flow stress has been found to be essentially independent of strain at least to the 3% strain limit used in this work.[26] Because of this n_b is zero and the rate sensitivity can be determined from discrete rate changes during each test. Although the lack of stress dependence of strain is not as well established for the high purity materials, it appears to be at least approximately true.

Tests were performed on specimens from three billets, 1339-41, at two temperatures, 1400 and 1450°C. Also, tests were conducted on 1.3 micron grain intercept hot pressed Al_2O_3 + 1/4% MgO which had been previously extensively tested.[27]

A typical load-deflection curve is plotted in Figure 3.6. Once steady-state stress was reached, it was customary to change $\dot{\epsilon}$ so that as many as four $\dot{\epsilon}$ - σ points were obtained for any one run.

The σ - $\dot{\epsilon}$ relations found for both the high purity Al_2O_3 and Al_2O_3 + 1/4% MgO are shown in Figure 3.7. Superimposed on this curve is corrected data (to the same stress factor) found for identical Al_2O_3 + 1/4% MgO billet tested in air at the same temperature.

The most extensive data was taken at 1400°C on the high purity Al_2O_3. The scatter was somewhat larger than expected from previous work on Al_2O_3 + 1/4% MgO. This suggested either the microstructure was variable from specimen to specimen or some apparatus problem, e.g., binding, was causing the variability.

The data obtained on Al_2O_3 + 1/4% MgO fits the earlier measurements remarkably well. This lends considerable confidence to the data on this new apparatus. The high purity samples are less plastic suggesting either that the effective grain size is larger than the Al_2O_3 + 1/4% MgO or creep is extremely sensitive to impurity content. This, of course, assumes that a major fraction of the creep process is due to diffusion as was found for less pure Al_2O_3.[27] Diffusion is known to be impurity dependent particularly in the region between extrinsic and intrinsic behavior, thus the deformation behavior may be a result of decreased diffusivity.

Fracture surfaces of crept and broken specimens were examined by electron microscopy techniques. It was found that grain growth had occurred. The average grain intercept had increased to 1.5 microns and a duplex structure which was on the verge of being apparent in the "as hot pressed" sample became obvious. The large grain areas had an intercept of 2.2 microns and the fine grain areas were 0.6 microns. The grain size increase explains some of the apparent creep resistance. The present data does not unequivocally answer the question of increased creep resistance due to purity. More extensive testing will enable a comparison with the existing creep data for Al_2O_3.

b. Grain Growth of Magnesia

Several grain growth experiments were conducted with samples of ~ 36 micron grain intercept high density MgO. The large starting grain size was chosen because only at this level was there anything approaching a normal distribution of grain size. Figure 3.8 illustrates the structure of the material studied.

Small samples were cut from three hot pressed billets; 1241, 1243 and 1244. Photomicrographs were taken in three areas for each billet and grain sizes determined by the linear intercept technique. Samples were annealed at 1300°C and 1500°C taking care to insure rapid heating and cooling for a series of times between 10 and 1000 minutes. Grain sizes were measured as before.

Grain growth could not be detected in the 1300°C anneals. There most certainly was some growth, but it was within the deviation of the linear intercept measurement. The large starting grain size played a role in the difficulty of detecting growth. The 1500°C data is shown in Figure 3.9. Also

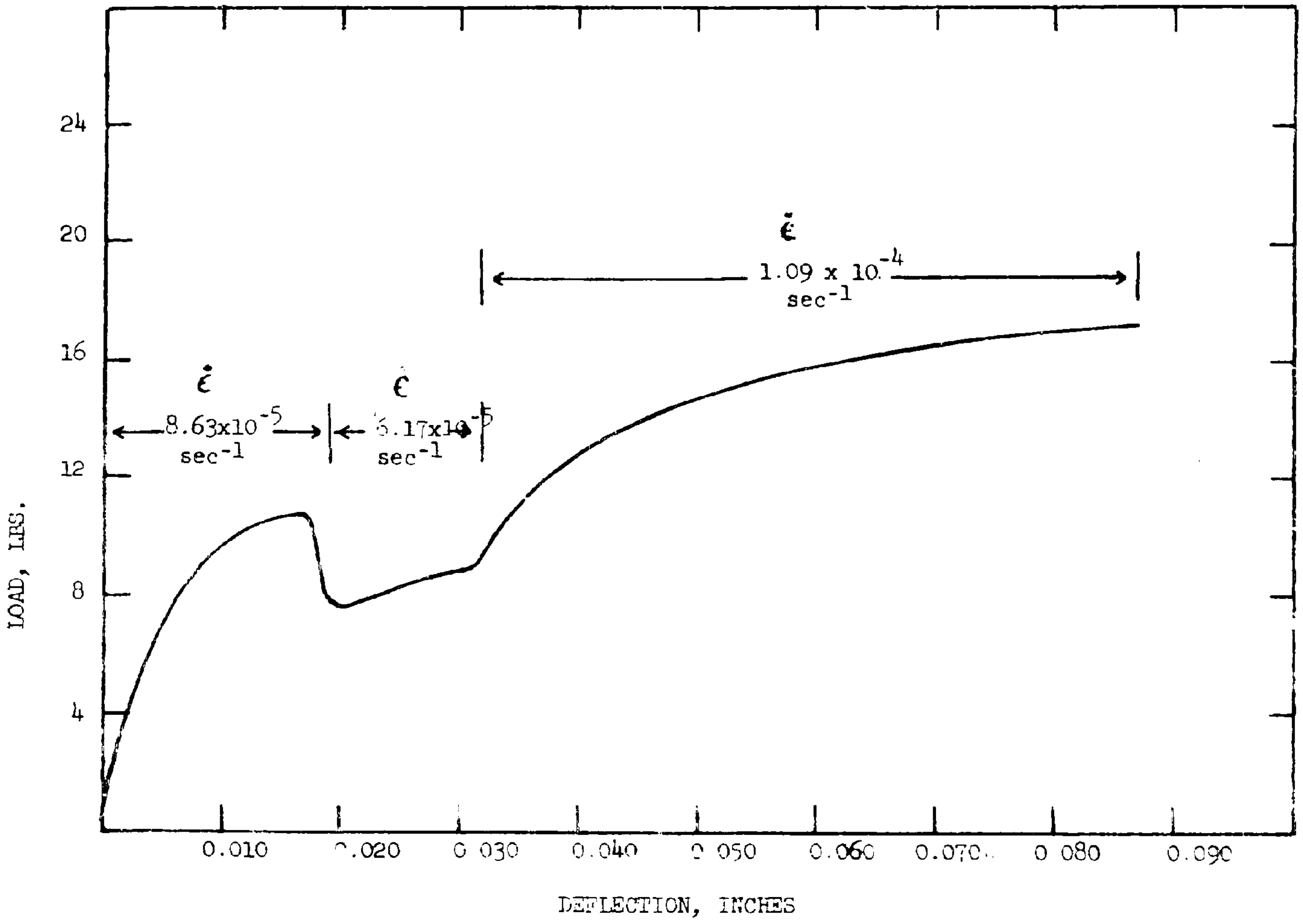

Figure 3.6 Load - Deflection Curve at Various Strain Rates for High Purity Al_2O_3

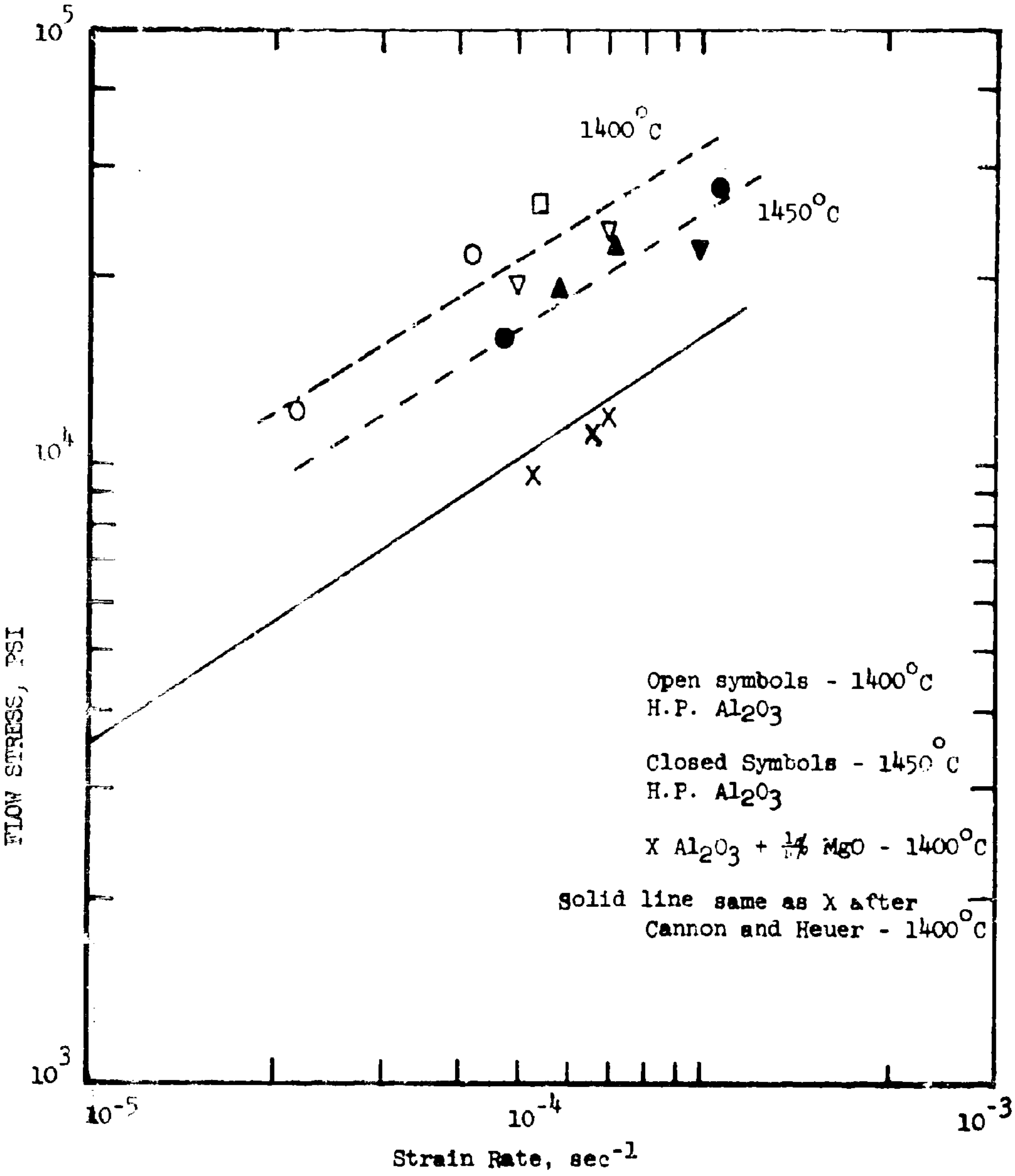

Figure 3.7 Steady-State Stress versus Strain Rate for High Purity Al_2O_3 and Al_2O_3 + 1/4% MgO.

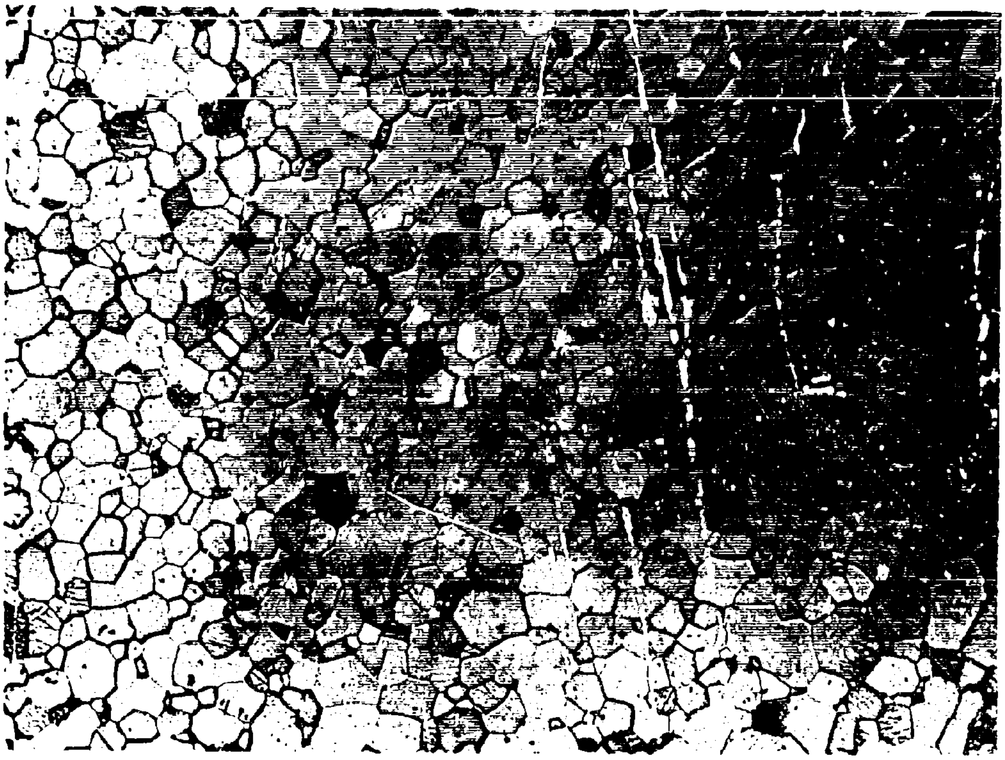

#5055 100X

Figure 3.8 Microstructure of High Purity MgO used for Grain Growth Study.

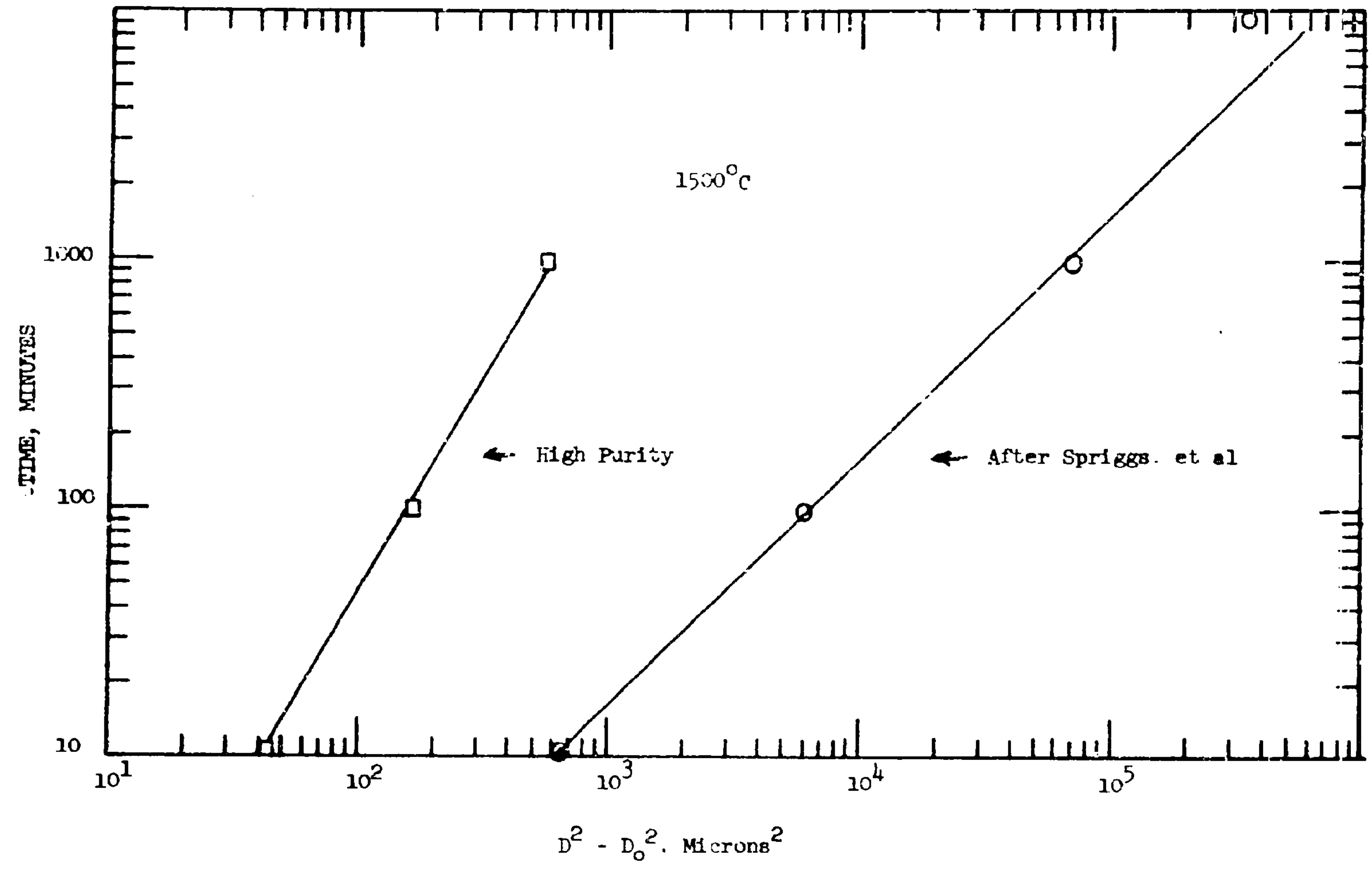

Figure 3.9 Grain Growth in High Purity MgO.

indicated on this plot is the data of Spriggs et al[30] for grain growth in 99.4% MgO (Fisher 300 M). The data is plotted according to the normal grain growth model of Turnbull[31]

$$D^2 - D_o^2 = (K \gamma V)t$$

where D = average grain diameter at time, t

D_o = original grain diameter at time zero

K = constant

γ = interfacial energy

V = gram-atomic volume

A plot of log D versus log t for the high purity gave a slope of 0.54 which is just slightly higher than the theoretical slope. Spriggs et al found a +1/2 slope, consequently, only a small difference exists. The main feature of the comparison is the difference in the constant terms. It appears that purity has a marked effect on grain growth in MgO, and further work to delineate and explain the process is warranted. However, this attempt will be hampered by an inability to fabricate small grain size MgO.

IV. PRESS FORGING ALUMINA

A. General

Studies have been conducted over the past several years on the press forging of Al_2O_3 and MgO.[1] Early work demonstrated that alumina single crystals having a volume up to 7 cm^3 could be grown in the solid state.[1,32] The apparent growth method was the strain-anneal technique which has been used to grow sizeable single crystals of metals. Implicit in this conclusion is that primary recrystallization is possible in polycrystalline Al_2O_3 having undergone a moderate strain rate deformation in the 1700-1950°C range.

Subsequent work[2-4,33] has substantiated that primary recrystallization occurs in Al_2O_3 forging. A highly elongated grain structure with the long axis of the grains normal to the pressing direction has been identified as a deformation structure. Upon primary recrystallization the microstructural texture is often absorbed, but a crystallographic texture which had accompanied the grain texture is retained. Also accompanying primary recrystallization and the equiaxed microstructure resulting from the process is a pore removal mechanism. It was suggested[33] that the porosity distributed throughout the structure presented preferred nucleation sites for the new generation of grains. This process itself could absorb porosity or the structure could be more susceptible to continued densification due to the nearness of pores to grain boundaries; their potential sink.

There are at least three potential motivations for forging Al_2O_3. They are, 1) the production of complicated shapes where a fine-grained dense microstructure is required, 2) improved mechanical properties due to the texture and retardation of structure sensitive failure mechanisms, and 3) high in-line optical transmission due to the crystallographic texture and the elimination of light scattering from birefringence. The mechanical properties have been studied extensively,[2] and it was found that the strength at -196°C and 1200°C was nearly independent of grain size in the 1-10 micron range. However, there was no apparent effect of texture on the mechanical properties between 1475-1700°C, the plastic range.[3] Some very interesting shape forging were accomplished last year;[3] namely, 60° cones and a near hemisphere were produced. Lack of explicit knowledge of the flow and failure criteria for the temperature interval (1800-1950°C) in which most of the forging is conducted prevented further major gains in shape forging. Improved in-line transmission has been the most dramatic outcome of the forging effort.[4] In-line light transmissions of 60% were achieved for the forged material as compared with a maximum of 20% for the best randomly oriented pore-free Al_2O_3 available at an equivalent thickness. The main limitations of the process were the extent of the transparent zone, complete pore removal and the extent of the crystallographic texture. The work to be described in the following sections was aimed toward solving the problems associated with producing transparent forged Al_2O_3. Also, some additional mechanical property data at -196°C and 1200°C at grain sizes > 10 microns were obtained.

B. Material and Procedure

The forgings were conducted with 99.97%, 0.3 micron Al_2O_3.* The powder is mainly alpha Al_2O_3, but it also contains 10-20% gamma Al_2O_3.

The forgings were conducted in a conventional induction heated graphite hot pressing furnace and press (Figure 4.1). CS graphite was used for the mold and sleeves while the pistons were made from ATJ graphite. The starting powder or billet conditions were arranged such that lateral flow was unrestricted during the deformation step. This was accomplished by either, 1) cold pressing the powder at 4 Kpsi in the graphite die and allowing unrestricted normal densification and shrinkage to occur during the heat up and dwell period prior to forging, or, 2) forging an undersized sintered (34-90% dense) or preforged (~99% dense) billet. One of the major variables in the study was the separating media between the graphite and Al_2O_3 billet being forged. This will be discussed in the next section. All forgings were conducted in an ambient atmosphere present with the essentially graphite systems. At 1860°C the atmosphere is expected to be C, CO, CO_2 with CO the major species.

C. Results and Discussion

The forging conditions and resulted are listed in Table 4.1. Runs 1042 and 1052 were conducted on the Al_2O_3 + 1/4% MgO alloy. High density specimens were forged to a 60% height reduction. The objective was to obtain large (>10 micron) grain size specimens to extend the grain size versus bend strength plots previously reported. The property results are given in Section IV C 2. The remaining forgings were concerned with the fabrication of transparent Al_2O_3.

1. Forging Studies

a. Lubrication and Reaction Barriers

---

* A. Meller Co., Providence, R.I., or Union Carbide, Chicago, Ill.

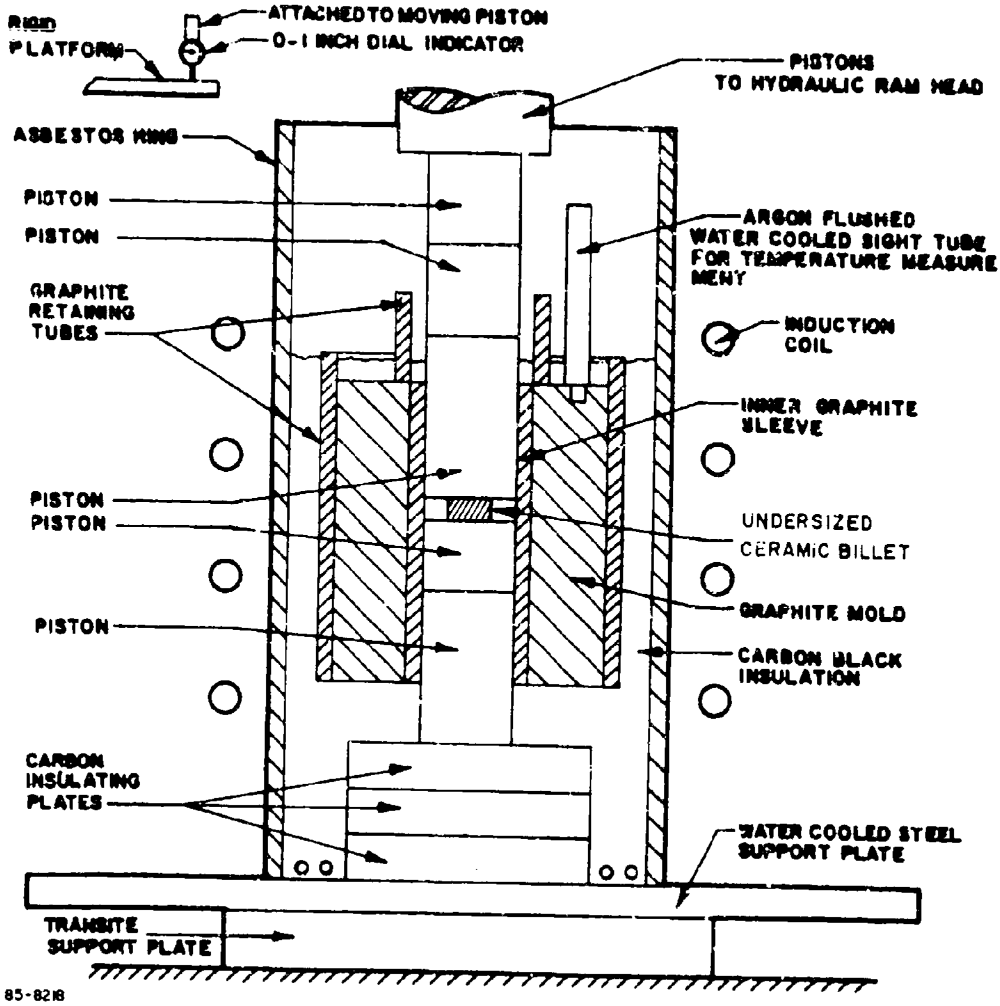

Figure 4.1 PRESSURE SINTERING APPARATUS USED FOR PRESS-FORGING EXPERIMENTS. NOTE THAT PRIOR TO FORGING, THERE IS NO CONTACT BETWEEN THE SPECIMEN AND THE DIE BODY

TABLE 4.1

FORGING CONDITIONS AND RESULTS

Billet No.	Powder Type	Separating Media	Forging Temp. °C	Heating Time min.	Final Press. psi	Time to Bring to final Pressure	Time to Zero Strain	Total Time at Temp. & Press.	Appearance
D1042	Al_2O_3 + ¼% MgO 99% dense	None	1880	60	2300	15	15	590	cracked - opaque
D1052	Same	M	1880	60	2300	10	2	178	cracked - opaque
D1110*	Ml-Al_2O_3	None	1870	120	5700	30	15	150	cracked - translucent
D1115A*	Ll-Al_2O_3	Mo	1840	95	4500	22	Piston broke		opaque
D1115B*	Ml-Al_2O_3	Mo	1840	95	4500	22			opaque
D1116*	Ml-Al_2O_3	Mo	1840	113	600	85	110	115	opaque center - translucent edge - large grains
D1118*	Ml-Al_2O_3	Mo	1840	79	7000	51	250	301	translucent. center seems darker
D1119*	Ml-Al_2O_3	Ta	1740	78	7000	55	75	305	reacted surface opaque
D1120*	Ml-Al_2O_3	Ta, Mo, BN, C	1840	80	7000	49	60	169	translucent under C and BN
D1122*	Ml-Al_2O_3	Mo top, C	1860	80	5600	45	2	47	piston broke, one side black
D1123	Ml-Al_2O_3	Mo-C top Mo-BN	1860	82	0			30	opaque. 2 1/2" dia.
D1125*	Ml-Al_2O_3	Bn top Mo-BN	1860	75	2800	11	75	75	translucent. uniform thickness

---

Ml = Adolf Meller Al_2O_3 Lot 68/182002B
Ll = Linde A

TABLE 4.1 (Cont'd)

FORGING CONDITIONS AND RESULTS

Billet No.	Powder Type	Separating Media	Forging Temp. °C	Heating Time min.	Final Press. psi	Time to Bring to find Pressure	Time to Zero Strain	Total Time at Temp. & Press.	Appearance
D1127*	M1-Al_2O_3	Mo-BN	1860	73	5600	13	120	120	uniform, translucent
D1129*	M1-Al_2O_3	Mo-BN	1860	71		6	62	62	
D1130	M1-Al_2O_3	BN	1860	77	0	0	0	0	34% dense
D1132***	M1-Al_2O_3 Presint. 37%	Mo-BN	1860	75	5100	10	45	60	very translucent and uniform
D1134*	M1-Al_2O_3	Mo-heavy BN	1860	75	5600	5	30	60	opaque center, translucent edge
D1135*	M1-Al_2O_3	Mo-BN	1860	75	5600	8	32	60	one face center opaque, rest translucent
D1136*	M1-Al_2O_3	TiB_2-BN	1860	73	5600	6	44	60	large opaque center area translucent rim
D1137	½ of D1134	Mo-BN	1860	47	5600	10	60	60	translucent region extended
D1139*	M1-Al_2O_3	Mo-BN	1860	40	5600	8	10	240	uniform, translucent
D1140*	D1129	Mo-BN	1860	47	5600	10	30	240	uniform, translucent large grains on faces
D1141*	M1-Al_2O_3 Presint. 57%	Mo-BN	1860	38	5600	10	60	60	repressed
D1142*	M1-Al_2O_3	Mo-BN	1860	42	5600	8	30	30	opaque center with large grains coming from interface

---

* 10-15 min. hold at temp. prior to pressure application

** forged into 4" dia - all other 3" die

TABLE 4.1 (Concl'd)

FORGING CONDITIONS AND RESULTS

Billet No.	Powder Type	Separating Media	Forging Temp. °C	Heating Time min.	Final Press. psi	Time to Bring to find Pressure	Time to Zero Strain	Total Time at Temp. & Press.	Appearance
D1143	M1-Al_2O_3 Presint. 78%	Mo-BN	1860	53	0	0	0	0	78% dense. delaminated
D1144	M1-Al_2O_3 Presint. 80%	Mo-BN	1860	45	5600	6	32	32	uniform translucent
D1151*	D1141	Mo-top Mo-BN	1860	37	5600	8	15	120	uniform translucent
D1153*	M1-Al_2O_3	Mo-top Mo-BN	1860	75	5600	6	24	120	translucent edges. slightly dark center
D1155	L1-Al_2O_3	Mo-BN	1900	79	0			75	60% dense
D1157	M1-Al_2O_3	Mo-BN	1900					15	
D1161*	D1157	Mo-BN	1880	35	5600	7	15	52	uniform translucent 4 cracks
D1164*	D1155	Mo-BN	1880	50	5600	8	30	90	dense but dark
D1167*	M1-Al_2O_3 Presint. 91%	Mo-BN	1880	40	5600	15	50	90	opaque
D1186	M1-Al_2O_3	3/8" BN plate	1880	130	5600	6	75	75	
D1187	M1-Al_2O_3	Mo-BN	1880	120	5600	5	36	36	opaque center. translucent edge
D1188*	M1-Al_2O_3	Mo-BN	1880	120	5600	10	81	81	uniform translucent

In the previous studies molybdenum was employed as a barrier layer between the graphite pistons and Al_2O_3. Graphite alone will reduce Al_2O_3 at these temperatures. Another common problem during the previous work was the forging of billets which ended up with a non-uniform cross section. This, of course, resulted in varying strain usually tappering from the center to edge with the edge receiving the greatest height reduction. The condition occasionally resulted in this strain gradient the critical strain for recrystallization was reached and nucleation of only a few grains occurred. (See references 4 or Aust's review article[34], for a complete discussion of the strain anneal process). This condition was clearly undesirable from the viewpoint of the desired uniform crystallographically oriented dense microstructure.

Runs 1119-1127, 1136 and 1186 were experiments with a variety of media as noted in Table 4.1. The metals employed were usually in the form of 0.010 inch thick foil; however, experiments with Mo ranged all the way from 0.005 to 0.125 inches. The material noted C was pyrolytic graphite paper, and resulted in a dark Al_2O_3. Figure 4.2 illustrates cross-sectional regions adjacent to and in the middle of forging 1122 which employed pyrolytic graphite paper on one face adjacent to the graphite paper which illustrates the great influence impurities have on grain growth and/or recrystallization. Ta was very bad and should not have been included due to the known reactivity. Some minor sticking occurred with TiB_2 and the billet cracked.

BN was usually employed as a sprayed powder coating either directly on the graphite mold or as a layer between Mo foil and Al_2O_3. Three-eighth inch thick BN plates were used in Run 1186, and both the plates and the Al_2O_3 billet cracked. The best material system devised was graphite piston, 0.010" Mo plate, and a BN sprayed powder wash. This resulted in many forged billets with both a uniform cross-section and uniform translucency. The cross-section variation on many billets was < 0.010". However, some specimens, e.g., 1142 and 1167 exhibited considerable doming even though this lubrication system was employed. It was clear, therefore, that the uniformity of a forged billet was also dependent on forging parameters.

b. Sintering During Initial Stage of Powder Forging

The runs listed in Table 4.2 describe the conditions and results of several experiments to delineate the initial stage of the powder forging cycle. It was common practice to cold press the powder at 570 psi. During the 1-2 hour heating to the forging temperature, the specimen sintered to some degree. It was also common practice to employ a 10-minute isothermal period prior to the initiation of forging. These runs isolate the condition of the blank prior to forging. Run FA 108 from a previous study[4] apparently sintered more readily than D1130. Both specimens were cold pressed at the same low pressure resulting in a low green density. Thus, the relatively low sintered density is not surprising, but the difference between the two is somewhat surprising. The only known variable in this study was the powder supply. Apparently Linde A sinters faster than Meller at this low green density. Runs D1155 and D1157 were conducted to verify this result and although the order remained the same, the difference became less. Slightly higher temperatures and longer times bring the sintered density for Meller powder equal to Linde powder. Thus, the M-Al_2O_3 powder forging conducted at 1860°C listed in Table 4.1

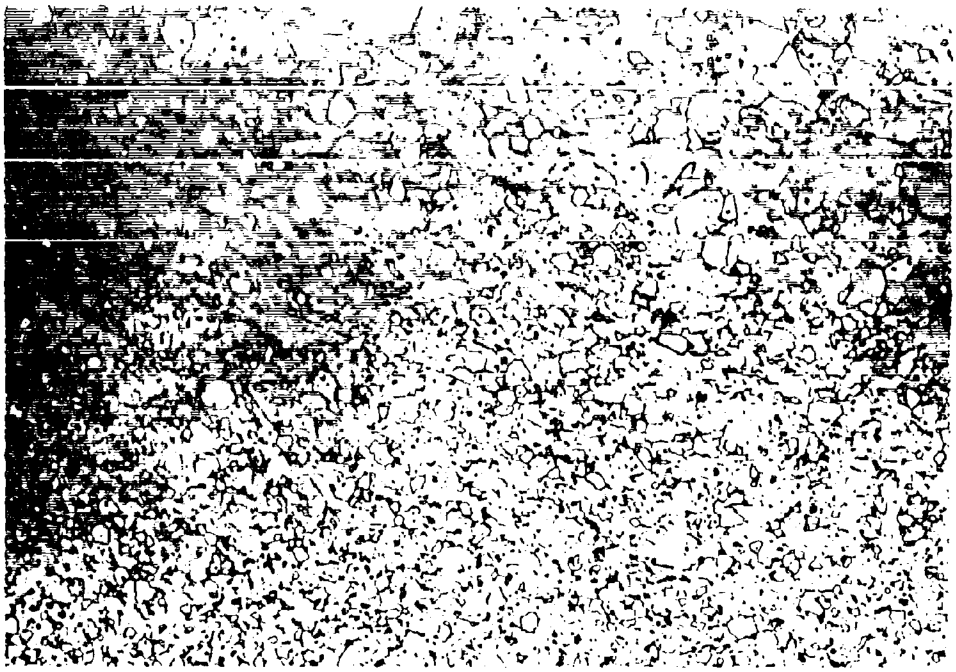

#5053-1 (a) 100X

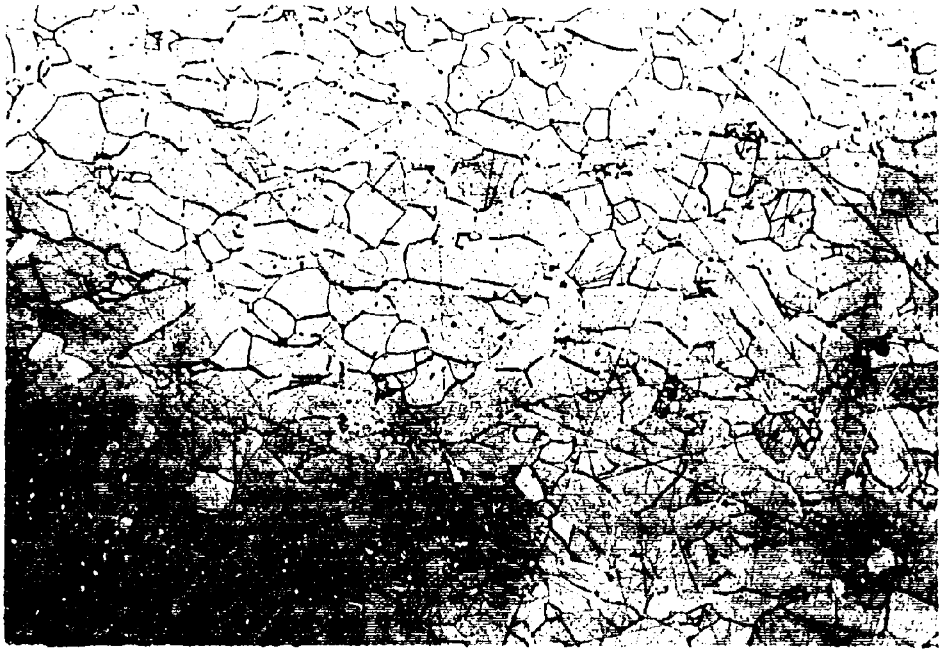

#5053 (b) 100X

Figure 4.2 Region Adjacent to Graphite Paper (a) and Central Region (b) in Billet 1122.

possessed the following conditions prior to the application of pressure and potential changes during forging:

density - 34%

diameter - 2.46 inches

length - 1.32 inches

potential area increase (based on 3" dia.) - 48%

potential height decrease (based on 3" dia.) - 36%

potential density increase - 66%

The 1880°C forgings potentially underwent somewhat greater dimensional changes.

TABLE 4.2

SINTERING DURING INITIAL STAGES OF FORGING

Specimen	Temp. °C	Time min.	Relative Density
FA 108*	1860	10	62%
D1130	1860	10	34%
D1155*	1900	15	51%
D1157	1900	15	54%

* Linde A powder. Others, Meller Al_2O_3.

c. Sintered Forging Blanks

A number of runs were conducted with blanks that were fabricated by standard sintering techniques which included the use of binders, etc. The binder was burned at 850°C and the specimens were sintered in H_2 at temperatures between 1300-1600°C to relative densities of 37% to 90%. It was thought that the atmosphere entrapped with the pores may play a role in the nucleation and/or pore removal process. Coble[5] has shown that some gases (namely H_2 and O_2) are more soluble in the Al_2O_3 lattice. Run 1132 was probably the most transparent forging to date, but it is not clear whether this is due to the H_2 presinter or the use of a 4" die and the greater height reduction and lateral expansion. None of the remaining forgings conducted on the H_2 presintered blanks looked particularly promising. It is thought that the mediocore results were due to other forging parameters than the starting blank.

d. Crystallographic Texture

The texture or degree of crystallographic orientation in forged materials is best determined by x-ray diffraction techniques. Such information, of course, is of great benefit in the interpretation of the forging studies.

Texture is completely described by the construction of a pole figure which shows the distribution of the orientations of the various crystallographic axes of the individual crystallites in the polycrystalline body relative to the axes of the forging process. However, for the purpose of evaluating relative degrees of orientation a simpler system was devised.

The diffraction pattern of a random (powder) sample was obtained. Values of f_0 (h,k,l) defined by the relation

$$f_0\,(h,k,l) = \frac{I\,(h,k,l)}{\sum\limits_{hkl} I\,(hkl)}$$

were calculated.

Similarly, values f (hkl) were calculated from the diffraction pattern of a forged specimen. The ratios $R(hkl) = \frac{f\,(hkl)}{f_0\,(hkl)}$ which give the relative intensity of reflection were calculated and are plotted in Figure 4.3 against the angle ϕ between the planes (hkl) and the basal plane.

In the case of a random (powder) sample R has the constant value of unity. In the case of a perfectly oriented sample, R is zero everywhere except at $\phi = 0$ where it has some large finite value. In the case of a distribution of orientation, in general, R will decrease monotonically from $\phi = 0$ to $\phi = 90^\circ$. The better the crystallites are aligned, the higher the intercept at $\phi = 0$ and the steeper the drop with increasing ϕ.

Sections were cut from two samples such that the faces examined were 5/16 inch and 1 inch from the center of the billet. This, of course, was performed to ascertain if there were differences in the deformation and texture that might be present due to the radial material flow pattern. Figure 4.4 shows this relation for D1142 which exhibited recrystallization of large grains approximately 1/3 of the distance from the center. Figure 4.5 exhibits the ratio for the similar two sections of D1140 which exhibited some large surface grains, but was quite uniform radially. The steeper slopes on the two curves for the center sections indicate that these regions were more perfectly oriented in both cases. This must be caused by the massive material flow in this area and the local bending moments which gave rise torotation of the basal planes.

The relative orientation of outer sections for the four representative billets examined, D1127, D1140, D1142, D1151 are compared in Figure 4.6. This comparison shows that D1127 has no orientation and that D1151 is the most highly oriented with D1140 and D1142 being intermediate cases.

e. Strain Rate

The initial forging experiments (1110-1129) were conducted under a variety of strain rates. Strain rate was actually controlled by altering the rate of load increase, thus the strain rate control was rather crude. However, many of the slow strain rate forgings were opaque and two (D1116 and D1118) contained remarkably large crystals indicating that the nucleation process was slow at a well-defined strain zone. It was thought that in the

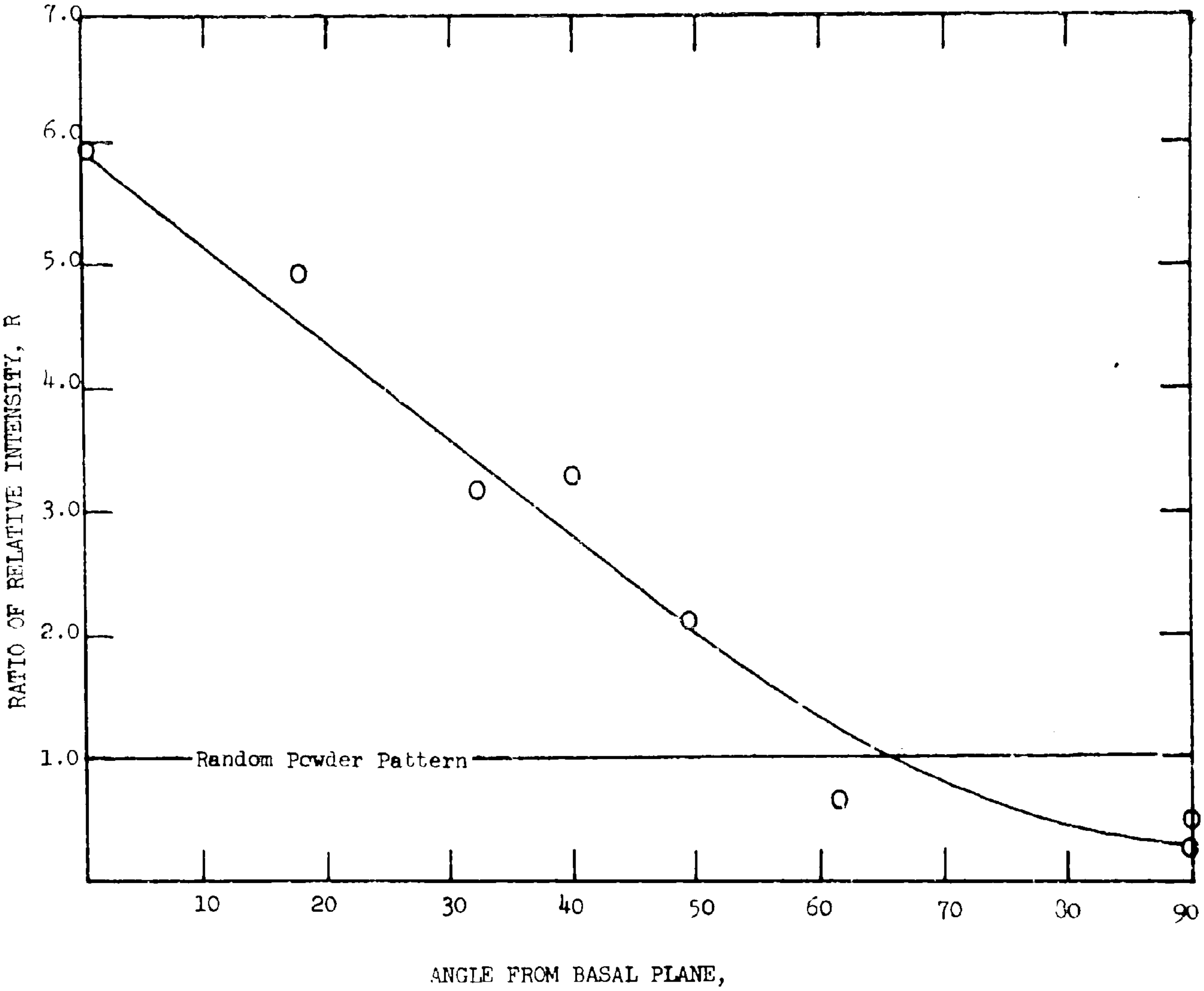

Figure 4.3 Ratio of Relative X-ray Intensity, R, for Forged D1142 over Powder Pattern versus Angle from Basal Plane

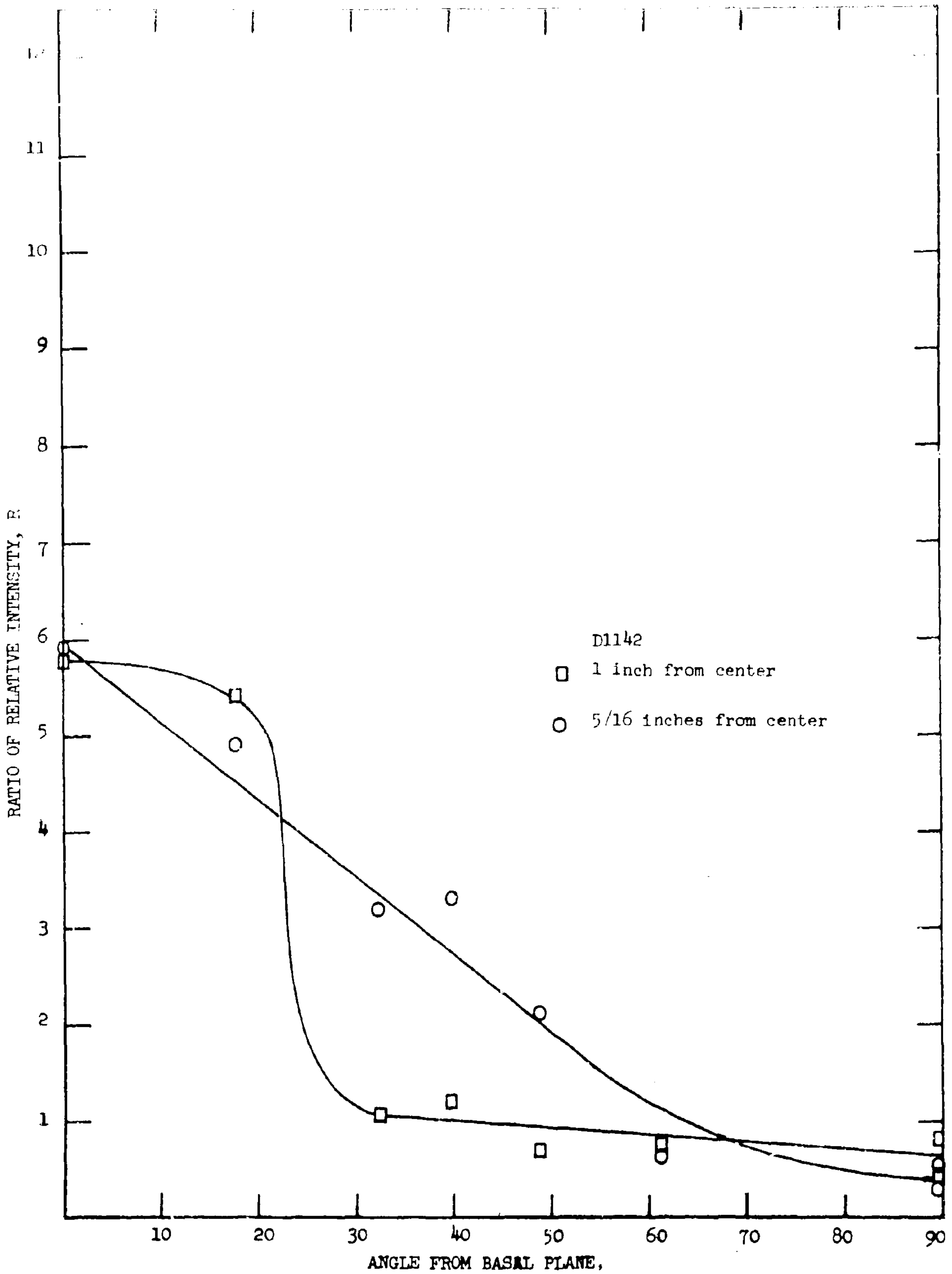

Figure 4.4 Ratio of Relative X-ray Intensity, R. for Forged D1142 at Center and Rim Position.

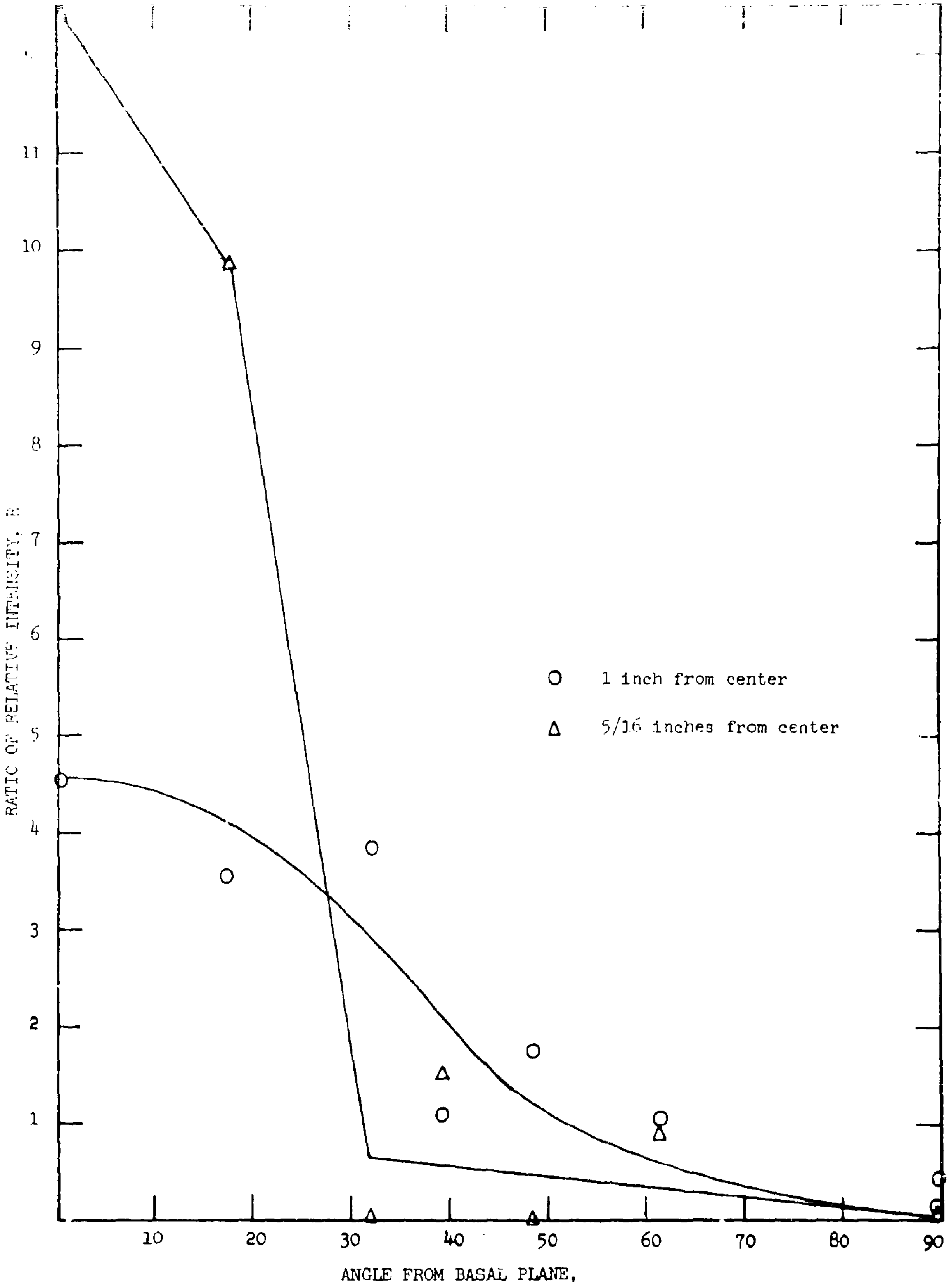

Figure 4.5 Ratio of Relative X-ray Intensity, R, for Forged 1140 at Center and Rim Position.

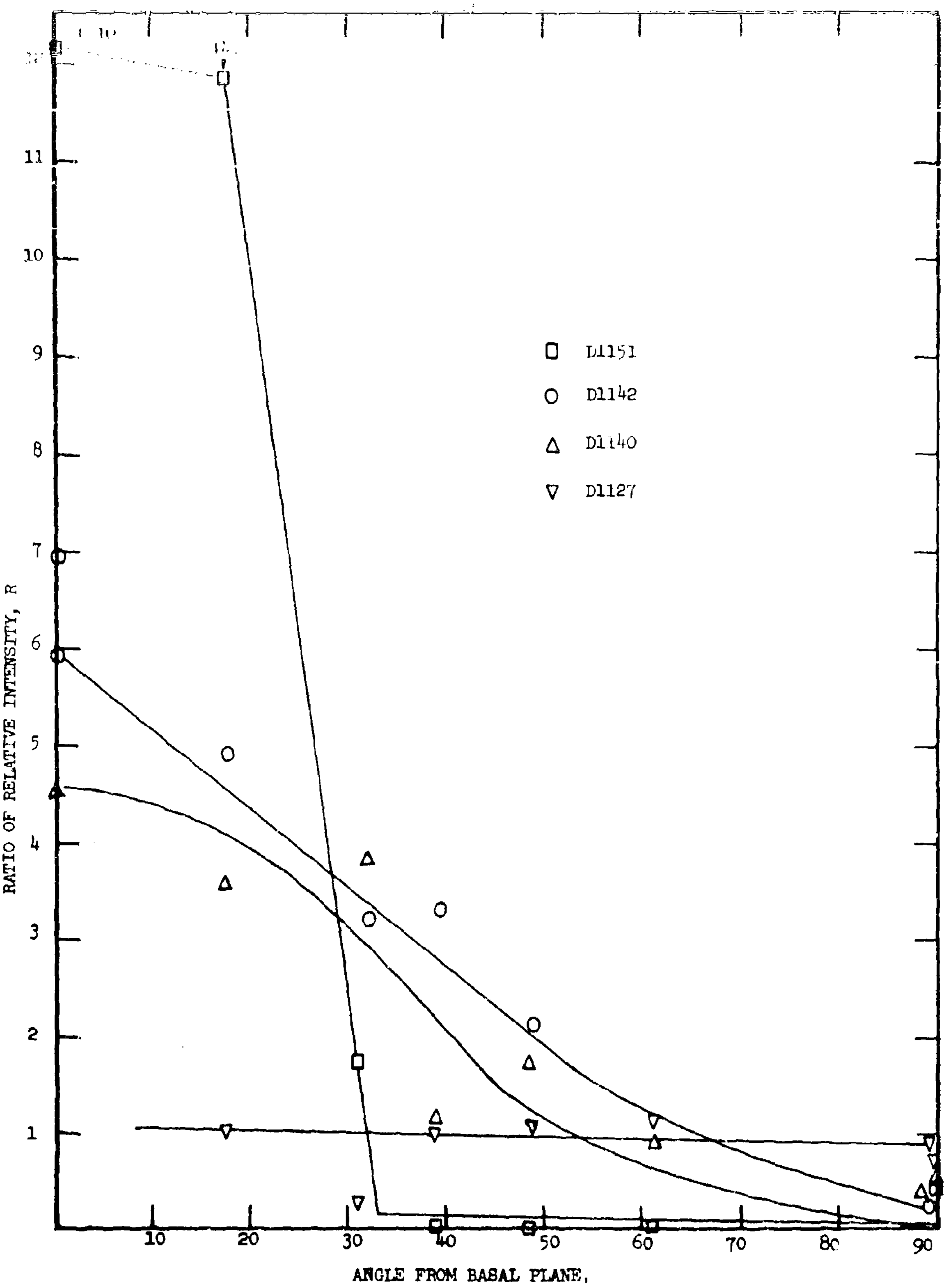

Figure 4.6 Comparison of X-ray, R, Values for Rim Position in Four Forged Al_2O_3 Samples.

process of the relatively slow deformation a critical strain for recrystallization was reached and maintained long enough for just a few strain free grains to nucleate and begin growth.

Runs conducted with a strain rate higher by as much as an order of magnitude exhibited more uniform microstructures which was thought to be due to a rapid transition through the critical strain level (approximately 5% strain).[4]

One run (1142) proved to be the exception to the above conclusion. This billet exhibited an equivalent level of large crystal growth to sample 1116. The interface between the large crystal and the fine grain recrystallized product is shown in Figure 4.7. This result may have been due to high frictional forces between the sample and barrier layer due to too thin a BN layer. It is not possible to be conclusive in the explanation of run 1142. It is interesting to note from the prior discussion on crystallographic texture that a marked orientation was present in the center section which presumably was only strained ~ 5% at the time recrystallization occurred. This implied that extensive deformation occurred after the nucleation of the large grains. As the center section did not appear to be recrystallized this also implies that the deformation texture is more perfect than the recrystallized structure.

f. Hold Period at Temperature and Pressure

The following discussion will consider only samples that were given the relatively rapid strain rate (full load in less than 15 minutes). The deformation process following the application of full load was monitored through a ram travel measuring system. There was a general trend for time to zero deformation to be directly related to the time of pressure application. In other words, a run in which 13 minutes was taken to bring the load to 5600 psi took 120 minutes before the piston movement halted whereas a 5 minute load application run took on the average 30 minutes before deformation was complete. A larger number of runs were conducted with a total hold period solely dependent on the time to zero strain; thus, the questions of hold period and strain rate are inter-related.

An example of the structure obtained for a slow strain rate and long hold period is shown in Figure 4.8 a and b. Figure 4.8 a, near the center of the billet possessed a structure representative of Al_2O_3 after ordinary hot pressing at high temperature. The tabular structure is probably due to anisotropic grain growth and the porosity entrapment is due to the exaggerated grain growth which has occurred in the course of the 2-hour deformation period. The outer 2/3 of a radial segment possessed a structure as illustrated in Figure 4.8 b. This segment of the billet was quite translucent as reflected by the low porosity level illustrated. It would appear that microstructural texture was present in this micrograph. However, the x-ray study showed no measureable crystallographic texture. Thus, it appears that either the slow rate of straining has caused a normal hot pressing condition for the bulk of the densification or recrystallization has removed any texture obtained during forging.

The structure shown in Figure 4.9 a and b represent the results of forging 1134 which had load and zero strain times of 5 and 30 minutes,

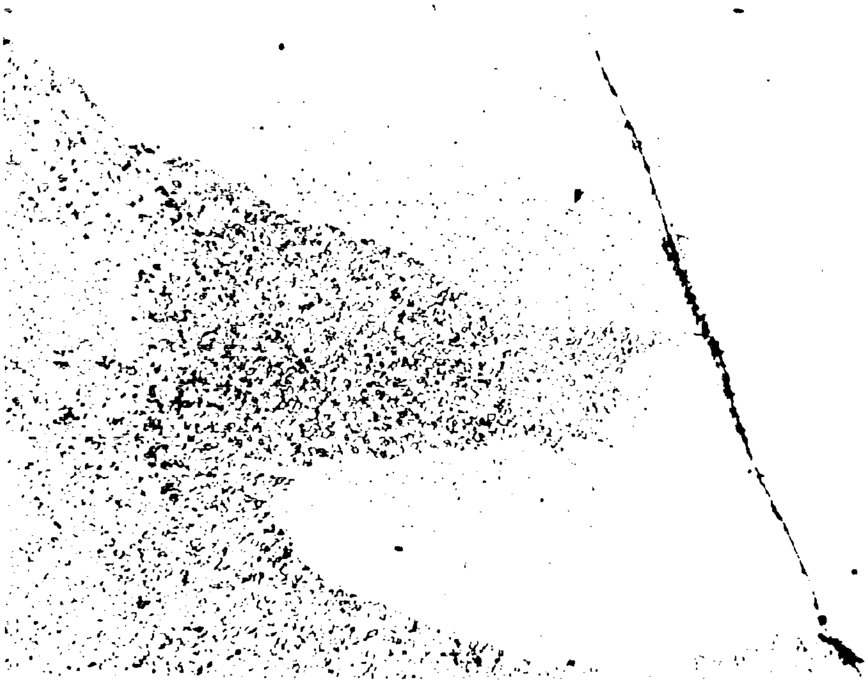

#5053-10 50X

Figure 4.7 Interface between Large Grain and Fine Grain Polycrystallized Structure.

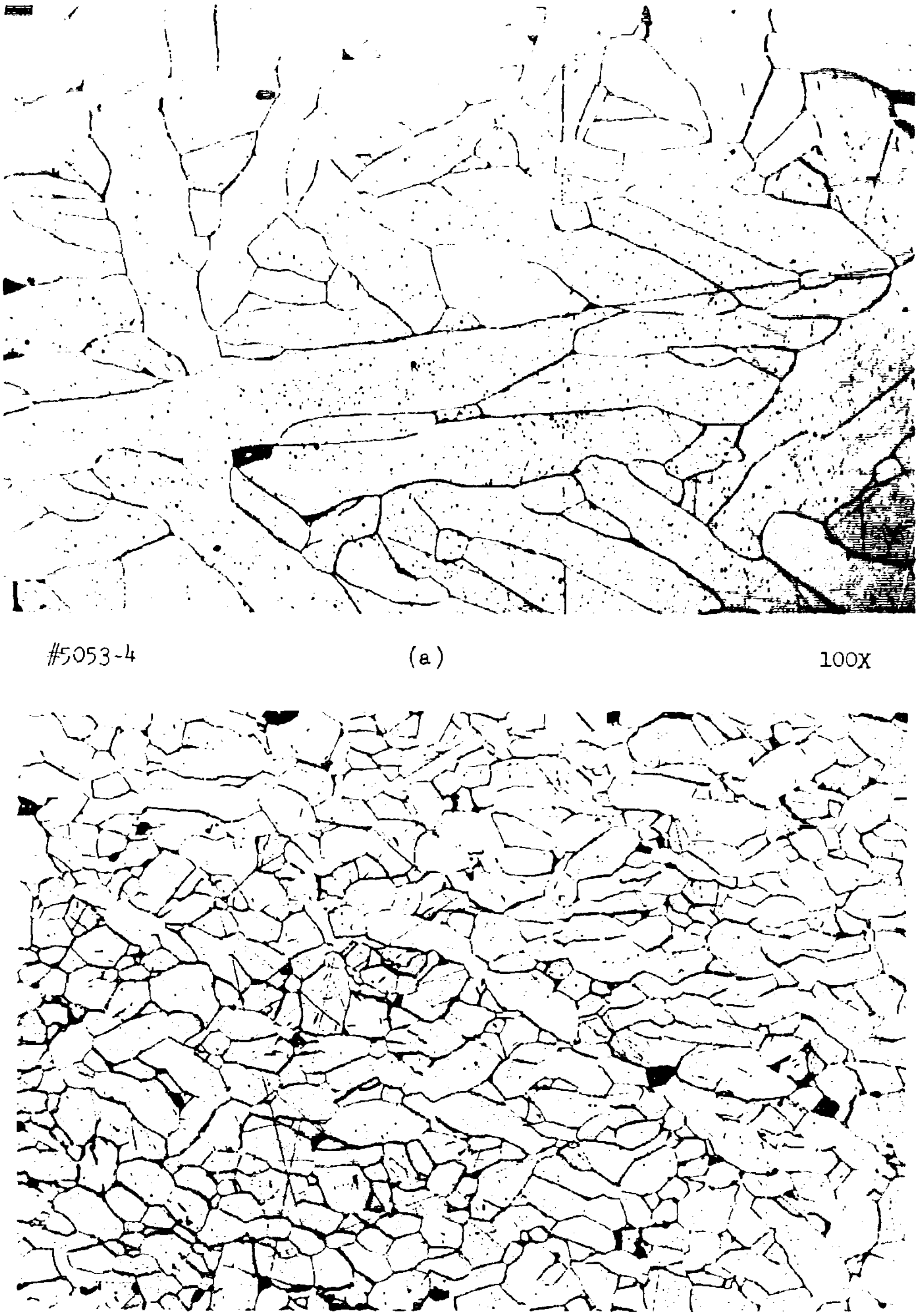

#5053-4 (a) 100X

#5053-5 (b) 100X

Figure 4.8 Areas near Center (a) and Edge (b) of Face Parallel to Pressing Direction for Billet 1127 Having Slow Deformation Cycle.

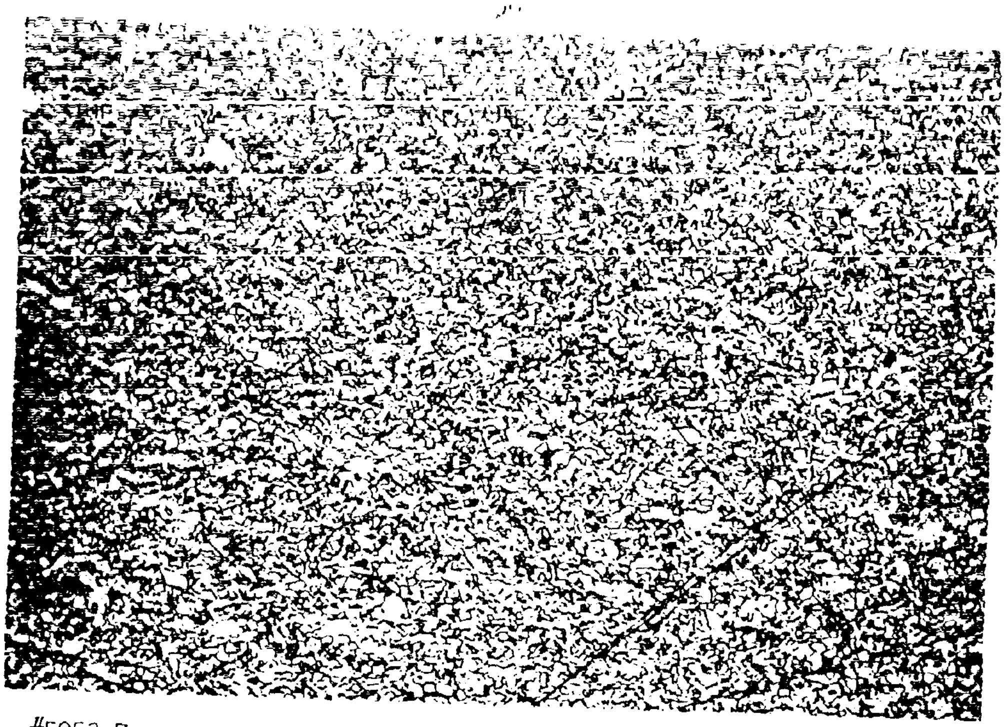

#5053-7

(a)

100X

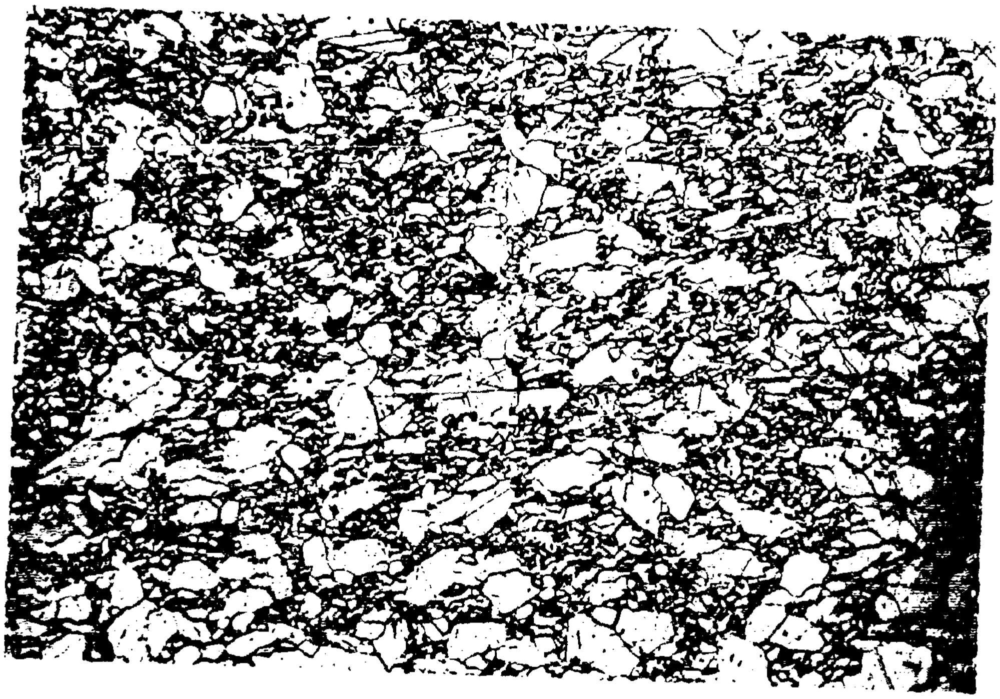

#5053-8

(b)

100X

Figure 4.9 Area Near Center (a) and Edge (b) of Face Parallel to Pressing Direction for Billet 1134 having Rapid Deformation Rate.

respectively. The central region was very fine-grained and possessed a small amount of porosity (it was slightly opaque). There does appear to be some microstructural texture although such texture does not become readily apparent at fine grain sizes in Al_2O_3.[2] Thus, this central region is probably unrecrystallized. Near the outer portions of the radius (Figure 4.9 b) a mixed grain size is apparent, and this region was considerably more transparent (pore free) than the central core. Apparently quite widely separated nucleation centers were formed and the recrystallized grain grew into the deformation structure. This would suggest that a relatively low amount of strain energy was in the lattice, and a level just slightly in excess of the critical strain was present in the periphery. It is interesting to note that recrystallization was accompanied by pore removal which is consistent with previous findings.[2,4,33] Thus, rapid deformation prevents a central "hot pressed structure," but at least in billet 1134 recrystallization was not complete.*

Billet 1140 was forged from a billet that had already been forged to high density. The billet was surface ground and cored to permit continued deformation. Deformation was complete in 30 minutes, but the sample was held under load for 240 minutes. Figure 4.11 illustrates the equiaxed structure which undoubtedly represents a recrystallization structure. It is also noteworthy that the grain size is markedly smaller than that observed for billet 1127 (Figure 4.8) which was at 1860°C for a considerably shorter time than 1140. This illustrates the grain refinement accompanying recrystallization (following high strains). Both billet faces (1140) exhibited very large grains. The present interpretation of this result is that ions from the separating media greatly enhanced normal grain growth. It would be difficult to prove that this was not associated with the deformation process itself however.

2. Properties

a. Mechanical

Four-point bend tests were performed on specimens cut normal to the pressing direction from forged billet 1052. Some grain size variation from center to edge was noted. By plotting the bend specimen location versus the grain size gradient, it was determined that the specimen gage length was between 16-20 μ grain intercept. Tests were conducted at 1200°C and -196°C for the purpose of extending to larger grain sizes strength-grain size measurement for forged Al_2O_3.

The strength-grain size plots for the two temperatures are shown in Figure 4.12 and 4.13. The -196°C tests indicate a slight fall-off in strength but not the normal $\sigma \sim G.S.^{-\frac{1}{2}}$ relationship often observed. The curve previously drawn to represent the strength-grain size curve at 1200°C would remain unchanged by the new data.

The results previously reported and discussed[3] led to the conclusion that the data did not support the view that basal slip or twinning nucleate fracture at -196°C or 1200°C.

---

* One-half of billet 1134 was reforged (1137) and the recrystallization zone was extended so that a region corresponding to Figure 4.9a possessed the structure shown in Figure 4.10. The translucent zone was also extended into the central region.

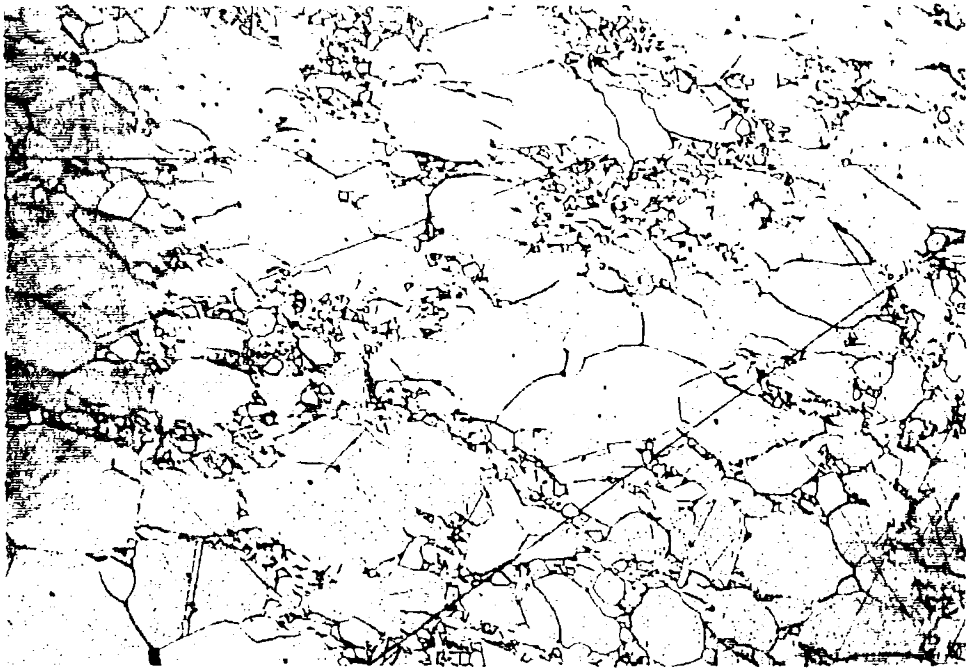

#5053-9 100X

Figure 4.10 Center Region of Billet 1137 (Reforged 1134) Showing Recrytsallization (corresponds to area in Figure 4.a).

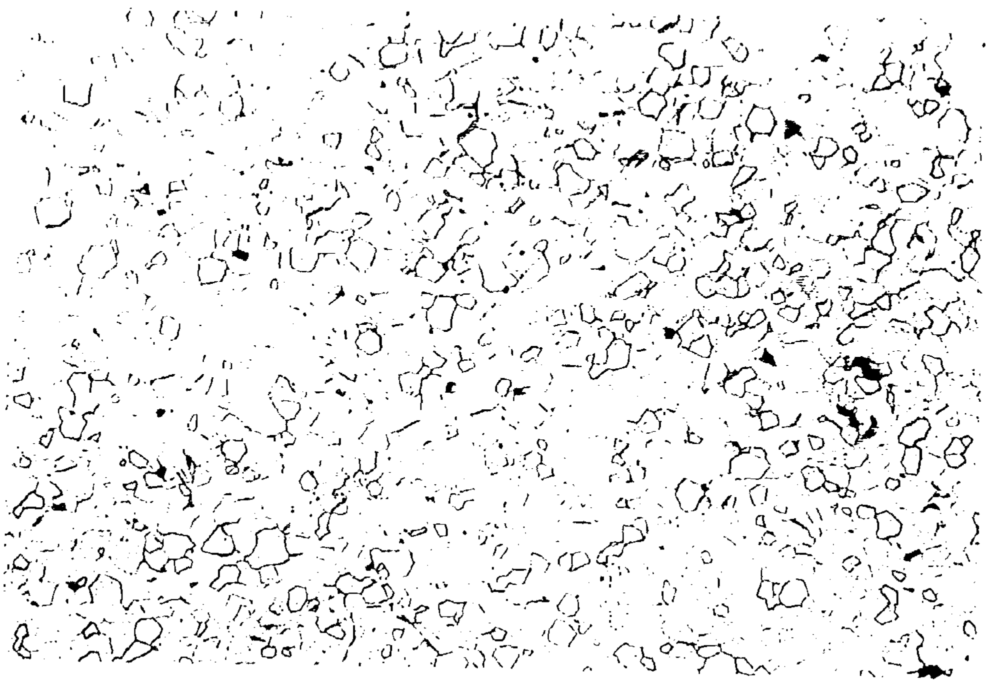

#5053-11

100X

Figure 4.11 Microstructure of Forged Billet D1140 Held at Temperature for 4 Hours.

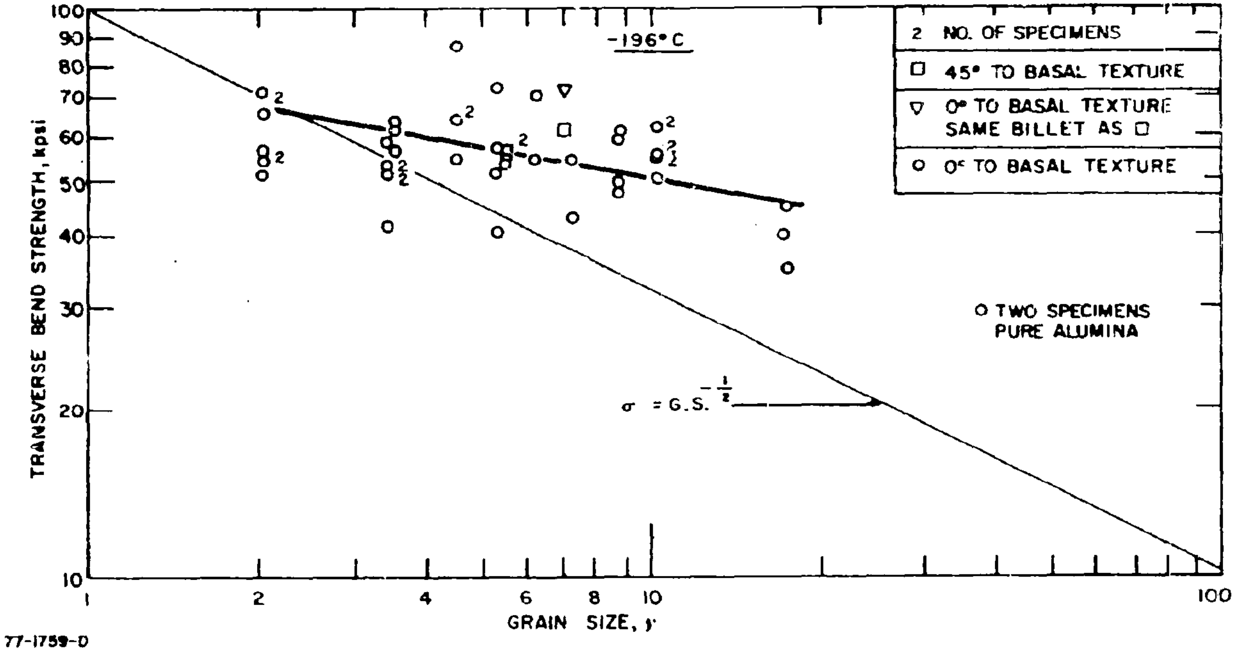

Figure 4.12 Bend Strength of Forged Alumina at -196°C.

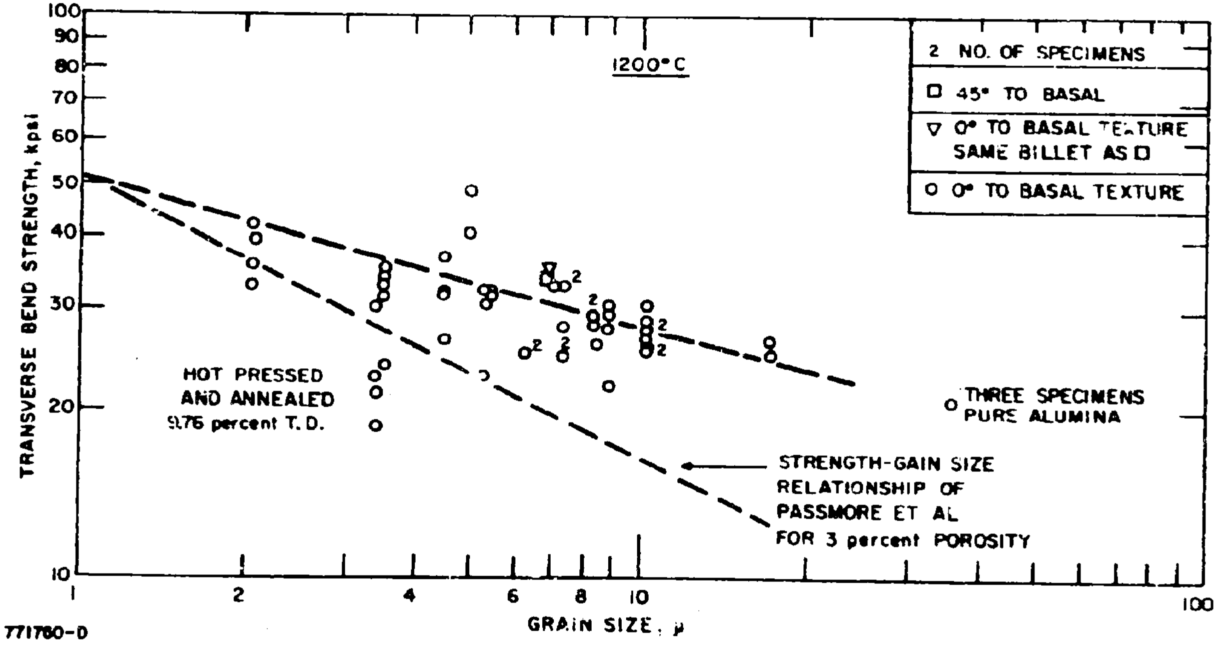

Figure 4.13 Bend Strength of Forged Alumina at 1200°C.

It was previously argued that the special grain boundary "character" was responsible for the decrease grain size dependence. This character was defined as structural characteristics such as atomic geometry, grain to grain orientation, boundary defect concentrations and chemical characteristics such as bonding impurities (to include entrapped gases). Because of the high degree of crystallographic orientation, the boundaries are probably of a very special structural character. That is, they probably have a predominant twist character with a very small tilt component. Flaws may interact in quite a different manner with this type of boundary as compared with a random boundary in Al_2O_3.

Kirchner[36] recently presented a paper where he correlated the slope of the strength-grain size curve with anisotropy in elasticity and thermal expansion of the system. Residual thermal contraction strains (after fabrication) result in stresses which degrade the strength properties of large grained highly anisotropic bodies (Al_2O_3, BeO, TiO_2) to a greater extent than a large grained nearly isotropic body (MgO). Removing the thermal expansion anisotropy by preparing a crystallographically oriented polycrystalline Al_2O_3 would tend to lower the grain size dependence by this model. This is precisely what has been observed. The authors now feel that this latter explanation is the major effect being observed in the strength properties of forged Al_2O_3.

b. Optical

Precise optical transmission data were not obtained during this program. A number of billets appear to possess low porosity levels and high crystallographic orientation, so measurements are warranted. Figure 4.14 gives a qualitative view of the transmission in billet D1151 which possessed the greatest basal orientation. The entire 3-inch diameter - 0.3 inch thick billet was of this quality. Billet D1132 measuring 3.4 inches diameter and 0.1 inches thick looks particularly promising and will be polished in a subsequent effort.

VI. SUMMARY

In contrast to moderate strain rate tests on MgO, dead load testing under H_2O displayed a classic stress corrosion curve. The activation volume and surface energy for the reaction interface were evaluated by the model of Charles and Hillig[20]. The values appeared quite reasonable when compared with those obtained for Al_2O_3. However, it was pointed out that a mechanical model similar to those invoked for metals may control the strength degradation as there exists plentiful evidence of dislocation controlled fracture in MgO. It was also pointed out that grain boundary impurities or discrete phases (sodium aluminum silicate) may be controlling stress corrosion. Alumina chemical polishing procedures were developed to extend a previous study on the effect of surface structure on fracture strength. Neither the "wet" or "dry" strength was significantly improved by chemical polishing. Only an annealed surface condition consistently showed strength improvements for Al_2O_3, and it was necessary to test in a corrosion free environment to demonstrate this phenomenon.

Dense high purity Al_2O_3 and MgO were fabricated. Successful fine grain size (<5 u) Al_2O_3 samples were generated and their brittle and plastic mechanical properties were determined. The brittle properties were equivalent

#5057 3 1/4X

Figure 4.14 Optical Transmission Through Forged Billet 1151.

to less pure hot pressed Al_2O_3. Increased creep resistance over less pure Al_2O_3 of a similar grain size was noted; however, it was not clear whether this was due to a small amount of grain growth which accompanied the test or decreased diffusivity due to the increased purity. All attempts to fabricate a uniform fine grain size high purity MgO failed due to the occurrence of exaggerated grain growth. Thirty micron uniform grain size material was fabricated and preliminary grain growth studies were conducted. Grain growth followed the normal growth law, but was about an order of magnitude slower than noted for less pure MgO.

Press forging studies were directed toward solving the engineering problems of forging. Along with this an understanding of the physical ceramics of primary recrystallization was gained. A mold lubrication system consisting of boron nitride sprayed on molybdenum plates was adopted. A rapid method of determining relative crystallographic orientation was developed and applied. Considerable understanding was obtained in developing a press forging cycle to control the deformation and recrystallization phenomena for the production of alumina with high in-line optical transmission. For example, it was found to be desirable to complete the first 10% of strain rapidly to inhibit the nucleation of large grains.

VII. REFERENCES

1. W.H. Rhodes, D.J. Sellers, T. Vasilos, A.H. Heuer, R.H. Duff and P. Burnett, "Microstructure Studies of Polycrystalline Refractory Oxides," NOw-65-9316f, Summary Report (1966).
2. A.H. Heuer, W.H. Rhodes, D.J. Sellers and T. Vasilos, "Microstructure Studies of Polycrystalline Refractory Oxides," NOw-66-0506-(d), Summary Report, (1967).
3. W.H. Rhodes, D.J. Sellers, R.M. Cannon, W.R. Mitchell and P. Burnett, "Microstructure Studies of Polycrystalline Refractory Oxides," N000-19-67-C-0336, Summary Report (1968).
4. W.H. Rhodes, D.J. Sellers, A.H. Heuer and T. Vasilos, "Development and Evaluation of Transparent Aluminum Oxide," N178-8986, Final Report June 1967.
5. W.B. Hillig, J. Appl. Phys., 32, 741 (1961)
6. J.J. Morley, P. Andrews and I. Whitney, Union Scientifique Continental du Verre Symposium (1961).
7. A.H. Heuer, Thesis, University of Leeds (1966).
8. F.J.P. Clarke, R.A.J. Sambell, and H.G. Tattersall, Phil. Mag., 1, 393 (1962).
9. G.E. Tomilovskii, Trudy Inst. Krist. Akad. Nauk. SSR, No. 8, 341 (1953).
10. A.G. King, in Materials Science Research, Plenum Press, New York, 1966, p. 529.
11. M.H. Leipold, "Impurity Distribution in MgO," J. Am. Ceram. Soc., 49, (9), 498-502 (1966).
12. A. Phillips, et al, "Electron Fractography Handbook," ML-TDR-64-416 (1965).
13. R.J. Charles, "Fracture," edited by Averbach et al, John Wiley and Sons, New York, New York, p. 225 (1959).
14. F.J.P. Clarke and R.A.J. Sambell, Phil. Mag., 5, 897 (1960).
15. R.J. Stokes and C.H. Li, J. Am. Ceram. Soc., 46, 423 (1963).
16. A.H. Cottrell, Introductory Lecture at the Fifth International Congress of the International Union of Crystallography, Cambridge (1960).
17. R. Rice, Contract No. NAS-7-726, Progress Report No. 14, October 1967.
18. A.R. Westwood, D.L. Goldheim and R.G. Lye, Phil. Mag., 16, 505 (1967).

VII. REFERENCES (Cont'd)

19. J.H. Westbrook and P.J. Jorgensen, Trans. AIME, 233, 425 (1965).

20. W.B. Hillig, R.J. Charles, from *High Strength Materials*, J. Wiley and Sons, New York (1965), p. 682.

21. R.J. Charles and R. Shaw, General Electric Report No. 62 R1 3081 M, (1962).

22. K.T. Aust and J.H. Westbrook, "Lattice Defects in Quenched Crystals," edited by Cotterell et al, Academic Press, New York. p. 771.

23. R.S. Gordon and W.D. Kingery, J. Am. Ceram. Soc., 49, 654 (1966).

24. E.R. Blosser, J.P.L. Contract No. 951578 (1968).

25. S. Timoshenko, *Strength of Materials*, Pt. II, 3rd edition, D. Van Nostrand, Princeton, p. 527 (1956).

26. A.H. Heuer and R.M. Cannon, Jr., "Plastic Deformation of Fine-Grained Aluminum Oxide," presented at U.S. AMRA Seminar on Structural Ceramics and Testing of Brittle Materials, March 28-30, 1967, IITRI, Chicago, to be published.

27. R.M. Cannon, Jr., and A.H. Heuer, to be published.

28. E.M. Passmore, R.M. Spriggs and T. Vasilos, J. Am. Ceram. Soc., 48, 1, 1965.

29. R.M. Spriggs, J.B. Mitchell, and T. Vasilos, J. Am. Ceram. Soc., 47, 323 (1964).

30. R.M. Spriggs, L.A. Brissette and T. Vasilos, J. Am. Ceram. Soc., 47, 417 (1964).

31. D. Turnbull, Trans. AIME 191, 661 (1951).

32. D.J. Sellers, A.H. Heuer, W.H. Rhodes and T. Vasilos, "Alumina Crystal Growth by Solid-State Techniques," J. Am. Ceram. Soc., 50, 217 (1967).

33. A.H. Heuer, D.J. Sellers and W.H. Rhodes, "Hot Working of Aluminum Oxide: I - Primary Recrystallization and Texture," to be published J. Am. Ceram. Soc., 1969.

34. K.T. Aust, in the *Art and Science of Growing Crystals*, John Wiley and Sons, New York, 1963, p. 452.

35. R.L. Coble, J. Am. Ceram. Soc., 45, 123 (1962).

VII. REFERENCES (Concl'd)

36. H.P. Kirchner and R.M. Gruver, The Grain Size Dependence of Strength in Ceramic Oxides, presented at Basic Science Meeting of Am. Ceram. Soc., October 1968.

37. R.W. Rice, Proc. of Brit. Ceram. Soc., p. 99 (1969).

Unclassified
Security Classification

DOCUMENT CONTROL DATA - R & D

(Security classification of title, body of abstract and indexing annotation must be entered when the overall report is classified)

1. ORIGINATING ACTIVITY (Corporate author)
Avco Corporation, Applied Technology Division
Lowell Industrial Park, Lowell, Mass. 01851

2a. REPORT SECURITY CLASSIFICATION
None

2b. GROUP

3. REPORT TITLE
MICROSTRUCTURE STUDIES OF POLYCRYSTALLINE OXIDES

4. DESCRIPTIVE NOTES (Type of report and inclusive dates)
Summary Report, 25 May 1968 to 24 June 1969

5. AUTHOR(S) (First name, middle initial, last name)
William H. Rhodes
Paul F. Jahn
Paul L. Burnett

6. REPORT DATE
24 June 1969

7a. TOTAL NO. OF PAGES
67

7b. NO. OF REFS
37

8a. CONTRACT OR GRANT NO.
N00019-68-C-0108

b. PROJECT NO.

c.

d.

9a. ORIGINATOR'S REPORT NUMBER(S)
AVATD-0121-69-CR

9b. OTHER REPORT NO(S) (Any other numbers that may be assigned this report)

10. DISTRIBUTION STATEMENT
This document is subjected to special export controls and each transmittal to foreign governments or foreign nationals may be made only with the prior approval of the Commander, Naval Air Systems Command.

11. SUPPLEMENTARY NOTES
None

12. SPONSORING MILITARY ACTIVITY
Naval Air Systems Command
Washington, D.C.

13. ABSTRACT

Dead load-time to failure studies on polycrystalline MgO exhibited a decreasing load bearing capacity with time which was interpreted by the Charles and Hillig stress corrosion model. The possibility of a mechanical model similar to that invoked for metals was considered and not ruled out.

Chemical polishing of polycrystalline Al_2O_3 was accomplished, but mechanical tests failed to show a statistically valid strength improvement. Only a thermally etched surface from an earlier study exhibited a pronounced surface sensitivity to fracture strength, and dry testing conditions were required to unequivocally demonstrate this effect.

Two new grades of high purity Al_2O_3 and MgO powders were fabricated, and mechanical testing of the Al_2O_3 showed equivalent brittle strengths and increased creep resistance when compared with less pure material with an equivalent microstructure. The explanation for the creep resistance may be either a slight increase in grain size which accompanied the test or decreased diffusivity due to the increased purity.

Preliminary grain growth studies on high purity MgO indicate a normal grain growth behavior, but about an order of magnitude slower rate than 99.4% MgO.

Press forging of polycrystalline Al_2O_3 was directed toward solving the engineering and process control problems of forging material with a high in-line optical transmission. Considerable progress has been made although the desired properties have not yet been obtained.

DD FORM 1473 1 NOV 65

Unclassified
Security Classification

Unclassified
Security Classification

14 KEY WORDS	LINK A		LINK B		LINK C	
	ROLE	WT	ROLE	WT	ROLE	WT
Alumina						
Magnesia						
Hot working						
Press forging						
Mechanical properties						
Stress corrosion						
Plastic deformation						
High purity						

Unclassified
Security Classification